Progress in Neurobiology 199 (2021) 101937

Contents lists available at ScienceDirect

Progress in Neurobiology

journal homepage: www.elsevier.com/locate/pneurobio

Original Research Article

Astrocyte-derived Wnt growth factors are required for endothelial blood-brain barrier maintenance

Sylvaine Guérit [a,1], Elif Fidan [a], Jadranka Macas [a], Cathrin Jaqueline Czupalla [a,2], Ricardo Figueiredo [b], Aruvi Vijikumar [a], Burak Hasan Yalcin [a,3], Sonja Thom [a], Peter Winter [b], Holger Gerhardt [c,d,e,f,g,h], Kavi Devraj [a,i], Stefan Liebner [a,j,k,*]

[a] Institute of Neurology (Edinger Institute), University Hospital, Goethe University Frankfurt, Frankfurt Am Main, Germany
[b] GenXPro GmbH, Altenhöferallee 3, 60438, Frankfurt Am Main, Germany
[c] Max Delbrück Center for Molecular Medicine, Berlin, Germany
[d] Vascular Biology Laboratory, London Research Institute – Cancer Research UK, Lincoln's Inn Fields Laboratories, London, England, UK
[e] German Center for Cardiovascular Research, Berlin, Germany
[f] Vascular Patterning Laboratory, VIB Center for Cancer Biology, Leuven, Belgium
[g] Vascular Patterning Laboratory, Department of Oncology, KU Leuven, Leuven, Belgium
[h] Berlin Institute of Health, Berlin, Germany
[i] Frankfurt Cancer Institute, Germany
[j] Excellence Cluster Cardio-Pulmonary Systems (ECCPS), Partner Site Frankfurt, Germany
[k] German Center for Cardiovascular Research (DZHK), Partner Site, Frankfurt/Mainz, Frankfurt, Germany

ARTICLE INFO

Keywords:
Wnt-signalling
Blood-Brain barrier
Astrocytes
Neuro-vascular unit
Barrier maintenance
Caveolae

ABSTRACT

Maintenance of the endothelial blood-brain-barrier (BBB) through Wnt/β-catenin signalling is essential for neuronal function. The cells however, providing Wnt growth factors at the adult neurovascular unit (NVU) are poorly explored. Here we show by conditionally knocking out the *evenness interrupted* (*Evi*) gene in astrocytes ($Evi^{\Delta AC}$) that astrocytic Wnt release is crucial for BBB and NVU integrity. $Evi^{\Delta AC}$ mice developed brain oedema and increased vascular tracer leakage. While brain vascularization and endothelial junctions were not altered in 10 and 40 week-old mice, endothelial caveolin(Cav)-1-mediated vesicle formation was increased *in vivo* and *in vitro*. Moreover, astrocytic end-feet were swollen, and aquaporin-4 distribution was disturbed, coinciding with decreased astrocytic Wnt activity. Vascular permeability correlated with increased neuronal activation by c-fos staining, indicative of altered neuronal function. Astrocyte-derived Wnts thus serve to maintain Wnt/β-catenin activity in endothelia and in astrocytes, thereby controlling Cav-1 expression, vesicular abundance, and end-feet integrity at the NVU.

1. Introduction

Since the establishment of the blood-brain barrier (BBB) concept by Max Lewandowsky (1900) and after coining the "BBB" term by Lina Stern and Raymond Gautier (1922) (reviewed by (Saunders et al., 2014)), astrocytes (ACs) at the neurovascular unit (NVU) have been considered as a major source of barrier-promoting factors (Cheslow and Alvarez, 2016; Liebner et al., 2011). In the last decade, the molecular structure of the BBB has been explored in great detail, and specifically the canonical Wnt/β-catenin pathway, mainly driven by Wnt7a, Wnt7b and the non-Wnt-related ligand norrin (Ndp), were shown to regulate angiogenesis as well as barriergenesis during development (Daneman et al., 2009; Liebner et al., 2008; Posokhova et al., 2015; Stenman et al., 2008; Vanhollebeke et al., 2015; Zhou and Nathans, 2014; Zhou et al., 2014a). It has been shown that during vertebrate embryonic development, Wnt factors are primarily secreted by neural precursor cells, fostering vessel growth and barrier formation (Daneman et al., 2009; Weidenfeller et al., 2007). Although vessels throughout the central

* Corresponding author at: Institute of Neurology (Edinger Institute), University Hospital, Goethe University Frankfurt, Frankfurt am Main, Germany.
E-mail address: stefan.liebner@kgu.de (S. Liebner).
[1] Current position:Normandie Univ, UNICAEN, INSERM U1237, serine protease and pathophysiology of the neurovascular unit, Centre Cyceron, Caen, France.
[2] Current position:450 E Jamie Ct, South San Francisco, CA 94080, USA.
[3] Current position:Abbott GmbH & Co. KG, Max-Planck-Ring 2, 65205 Wiesbaden, Germany.

https://doi.org/10.1016/j.pneurobio.2020.101937
Received 20 March 2020; Received in revised form 28 August 2020; Accepted 19 October 2020
Available online 28 December 2020
0301-0082/© 2020 The Author(s). Published by Elsevier Ltd. This is an open access article under the CC BY-NC-ND license (http://creativecommons.org/licenses/by-nc-nd/4.0/).

nervous system (CNS) develop barrier characteristics, with exception of the choroid plexus (CP), the circumventricular organs (CVOs) and to some extent the subventricular zone (SVZ), their properties and the molecular endowment was shown to be highly site-specific within the CNS (Benz et al., 2019; Saubaméa et al., 2012; Wang et al., 2010). With regard to the Wnt/β-catenin pathway, the retina, the olfactory bulb and the cerebellum utilize Ndp as the major ligand driving β-catenin signalling *via* a receptor complex formed by frizzled 4 (Fzd4), low-density lipoprotein receptor-related protein 5 (Lrp5), and tetraspannin 12 (Tspan12) (Chang et al., 2017; Eubelen et al., 2018; Vallon et al., 2018).

In the developing CNS, neural precursor cells are considered the major source of Wnt pathway-activating factors and blood vessels were shown to acquire, yet premature, BBB properties by ~E15 (Daneman et al., 2009; Lippmann et al., 2011; Stenman et al., 2008; Weidenfeller et al., 2007). Radial glia, which are present at the time point of neuroectodermal angiogenesis, have crucial function in angiogenic processes by secreting pro-angiogenic factors like VEGF and CXCL4 as well as the barrier-promoting factor retinoic acid (Cheslow and Alvarez, 2016). However, they appear to inhibit Wnt pathway activation in ECs, suggesting that they have functions other than secreting Wnt factors (Ma et al., 2013). Although the recent reports strongly suggest that BBB induction takes place far before astrocyte differentiation, it has also been shown that the maintenance of BBB function requires continuous β-catenin transcriptional activity (Zhou et al., 2014b).

Although more recently pericytes (PCs) have been shown to promote barrier properties in ECs *in vivo* and *in vitro*, for decades, ACs have been the prime suspects to secrete factors relevant for BBB maintenance (Haseloff et al., 2005; Janzer and Raff, 1987). Interestingly, as recently shown by Vanlandewijck as well as by Zhang and colleagues, pericytes do not express Wnt7a/Wnt7b whereas ACs appear to be the CNS cell type predominantly expressing these barrier-relevant growth factors in the adult mouse brain (Vanlandewijck et al., 2018; Zhang et al., 2014). Nonetheless, formal proof on the nature and function of these barrier-inducing factors is still missing. Specifically, since identification of the Wnt/β-catenin pathway as the key driver of barrier formation, it has not systematically been explored, which Wnt factors are released by ACs and if they contribute to BBB maintenance *in vivo*.

In order to tackle this question, we have conditionally deleted the Wnt secretion mediator *wntless* (Wls), also known as *evenness interrupted* (Evi) or Gpr177, in ACs (Bänziger et al., 2006). Cre recombinase expression was driven under the constitutively active human glial fibrillary acidic protein (hGFAP) promoter, leading to the deletion of the floxed Evi gene (Bajenaru et al., 2002; Carpenter et al., 2010).

Here we show that mice harbouring the conditional Evi deletion ($Evi^{\Delta AC}$) are alive, viable and born in the expected mendelian ratio, showing no gross morphological and behavioural phenotype compared to littermate controls (Evi^{Ctrl}). We did not observe significant changes in vessel morphology regarding vessel density and branching as well as extracellular matrix (ECM) distribution, despite decreased expression of Wnt pathway target genes in ECs. However, $Evi^{\Delta AC}$ exhibit a mild brain oedema and increased fluorescent tracer extravasation at 10 and 40 weeks of age, partially correlating with downregulation of junction genes like VE-cadherin/Cdh5 and zonula occludens-1/Tjp1 at 40 weeks, whereas junction morphology and function was unaffected. Instead, the frequency of endothelial vesicles and caveolin-1 (Cav-1) expression was significantly increased in $Evi^{\Delta AC}$ mice. In line with the hampered endothelial barrier function, 40-week-old $Evi^{\Delta AC}$ mice showed altered coverage of brain capillaries by astrocytic end-feet, evidenced by aquaporin-4 (Aqp4) staining. Moreover, electron microscopy revealed significant swelling of astrocytic end-feet in $Evi^{\Delta AC}$ mice, suggesting a cell-autonomous role of astrocytic Wnt factors *via* an autocrine pathway.

2. Material and methods

2.1. Animals

Animals were housed under standard conditions and fed *ad libitum*. All experimental protocols, handling and use of mice were approved by the Regierungspräsidium Darmstadt, Germany (V54−19c20/15-FK/1052). The transgenic mouse strains used in the project include hGFAP-Cre (Bajenaru et al., 2002), $Evi^{flox/flox}$ (Carpenter et al., 2010) and $Rosa26^{mT/mG}$ (The Jackson Laboratory, #007,576) (Muzumdar et al., 2007).

2.2. In vivo permeability assessment

2.2.1. Wet/dry assay

In order to assess the water content of the CNS tissue in our model, we performed a wet/dry experiment (Armulik et al., 2010). After anaesthesia (Ketamine 100 mg/kg, Xylazine 10 mg/kg), adult animals (10–20 weeks) were transcardially perfused with HBSS 1X during 5 min. Tissues were collected in 2 mL Eppendorf tubes and immediately weighed. After 6 days at 62 °C (open tubes), tissues were weighed again. Ratio between wet and dry tissue was calculated, as a well as the ratio of wet brain tissue to body weight. Data were compared using the Mann and Whitney test.

2.2.2. Tracer permeability

A mixture (1:2) of 2 mM Texas Red 3 kD dextran (TXR, #D3328, Invitrogen) and 5 mM fluorescein-5-thiosemicarbazide 0.42 kD (FTSC, #F121, Molecular Probes) was injected intravenously in anesthetized adult animals (10–20 weeks; 100 µl/25 *g* mouse) and allowed to circulate for 5 min as described in Devraj et al. (Devraj et al., 2018). After atrial puncture, 200−300 µL of blood was collected from the chest cavity (Micro tube Z-gel, #41.1500.005, Sarstedt) and thereafter, mice were immediately transcardially perfused for 3 min with PBS. Brain (cortex/subcortical area and cerebellum without hindbrain), spinal cord, liver and kidney as well as serum were collected and stored at −80 °C. On the day of fluorescence measurement, samples were thawed on ice, weighed and homogenized in PBS (300 µL for cortex, kidney and liver, 100 µL for spinal cord and cerebellum). Samples were centrifuged for 20 min, 4 °C at 15,000 *g*, and 40 µL of the supernatant or serum (1:4 dilution in PBS) were loaded on 384 well plate and fluorescence emissions (relative fluorescence units, RFU) were measured in a microplate reader (Tecan Infinite® 200 PRO, Switzerland) at excitation/emission wavelength of 595/625 nm for TXR dextran and 490/520 nm for FTSC. Sham animals (injection of PBS without tracer) were used to subtract auto-fluorescence values from the tissue and serum. Permeability index was calculated as follows: *Permeability Index* (mL/g) = *(Tissue RFUs/g tissue weight)/(Serum RFUs/mL serum)*. Data were compared using a *t*-test for each tissue independently.

For qualitative tracer leakage assessment, Alexa555®-Cadaverin was injected intravenously in anesthetized 10- and 40-week-old mice (2.5 mg/mL, 50 µl/25 g mouse, #A30677, Thermo Fisher Scientific) and allowed to circulate for 5 min. To make sure that the same amount of tracer was injected in all animals, blood was collected as described above and subsequently, mice were transcardially perfused for 3 min with PBS. Tissue was fixed in 4% PFA overnight at 4 °C and vibratome sections were cut thereafter at 50 µm thickness. For blocking and permeabilization, the tissue was incubated overnight (10% NDS, 0.1% Triton-X100 in PBS). Primary antibodies (Table 1) were incubated for 24 h and secondary for 4 h in antibody incubation buffer (1% BSA, 0.1% Triton-X100 in PBS). Sections were imaged either on a Nikon C1si confocal microscope (Nikon Instruments, Inc., Düsseldorf, Germany).

2.3. Isolation of mouse brain microvessels (MBMVs)

To investigate possible age-related differences, experiments were

Table 1
Antibodies for immunohistochemical staining on MBMVs, cryo- and vibratome sections.

Antibody	Marker for	Company	Catalog #	Dilution	Method
AQP4	AC end-feet	EMD Millipore	AB 2218	1:200	PFA
β-galactosidase		Abcam	AB616	1:500	PFA
Caveolin-1	vesicles	BD Bioscience	#610,059	1:200	MetOH
CD13/ Amino-peptidase N	PC	R&D System	AF2335	1:200	PFA
CD31	EC	BD Pharmingen	#553,370	1:100	PFA
Cdh5/VE-cadherin	EC junction	Santa-Cruz Biotechnology	sc-6458	1:100	MetOH
c-fos (H-125)	neuronal activation	Santa-Cruz Biotechnology	sc-7202	1:1000	PFA
Cldn5	brain EC junction	Thermo Fisher Scientific	#341,600	1:200	MetOH
Collagen IV	basal lamina	Bio-Rad	2150−1470	1:400	MetOH
Desmin	PCs	Dako	M0760	1:200	PFA
GFAP	AC cytoplasm	Abcam	AB53554	1:500	PFA
Glut-1 (C-terminal)	BBB ECs	Ian A Simpson (Devraj et al., 2011)	Rb serum	1:300	MetOH
Lama2	AC ECM	Abcam	AB11576	1:200	MetOH
Lama4	EC/PC ECM	Lydia Sorokin	377 (Rb serum)	1:1000	MetOH
Lama5	EC/PC ECM	Lydia Sorokin	4G6 A2 11 (R monoclonal)	Hybridoma SN, undiluted	MetOH
Podocalyxin (Podxl)	luminal EC membrane	R & D Systems	AF1556,	1:100	PFA/ MetOH
tomato-lectin	luminal EC membrane	Vector laboratories	DL-1178 (Alexa 649)	80 µL/mouse	
Donkey α-goat DyLight 550		Thermo Fisher Scientific	SA5−10087	1:500	
Donkey α-goat DyLight 650		Thermo Fisher Scientific	SA5−10089	1:500	
Donkey α-rabbit DyLight 488		Thermo Fisher Scientific	SA5−10038	1:500	
Donkey α-rabbit DyLight 550		Thermo Fisher Scientific	SA5−10039	1:500	
Donkey α-rat DyLight 550		Thermo Fisher Scientific	SA5−10027	1:500	

performed on both young adult (10 weeks) and middle-aged adult (40 weeks) mice. After cervical dislocation, brains were isolated and rolled on a sterile Whatman filter membrane (Schleicher & Schuell, Germany) to peel off meninges. They were subsequently homogenized in MBMV buffer (Fisher et al., 2007) using a dounce homogenizer (0.025 mm clearance, Wheaton, DWK Life Sciences) and centrifuged at 400 *g* for 10 min at 4 °C. The pellet was resuspended in 25% BSA and centrifuged at 2000 *g* for 20 min to remove myelin fat. The microvessel pellet containing also red blood cells and other single cells was resuspended in MBMV buffer and filtered through a 40 µm nylon mesh (#352340, Corning). For staining analysis, 5 µL of vessel suspension were deposited on fibronectin-precoated slide and fixed with 4% PFA for 5 min. For protein analysis, microvessels (from the top of the mesh) were resuspended in HES buffer (250mM sucrose, 20mM HEPES pH 7.4, 1 mM EDTA) (Devraj et al., 2011) with protease and phosphatase inhibitors (#4693159001 and #4906837001, respectively; Merck, Germany), sonicated (3 times 5 s, at 10% intensity; Bandelin Nanopuls equipped with an MS72 probe, Bandelin electronic GmbH & Co. KG, Germany) and stored at −80 °C. For RNA expression analysis, the microvessels were lysed in RLTplus buffer (RNeasy Plus Micro kit, #74034, Qiagen, Germany) and stored at −80 °C until use.

2.4. RT and qRT-PCR

RNA isolation was performed using the RNeasy plus Microkit (Qiagen) according to manufacturer's recommendations. For MBMVs analysis, 200 ng of RNA were used to generate cDNA (RevertAidTM H minus first strand cDNA synthesis kit, #K1632, ThermoScientific). For regular cell culture sample and whole brain, 500 ng of RNA were used.

Reverse Transcriptase PCR (RT-PCR) was performed on cDNA from cultured ACs using the Platinum™ Taq DNA polymerase (#11304011, Thermofisher) and the primers listed in Supplementary Table 1. Reference gene was G6pdx and RNA from mouse embryo E14.5 was used as positive control of amplification. RT-PCR products were loaded on 1.5% agarose gel and pictures were taken with a MultiImage™ Light Cabinet (FluorChem, Alpha Innotech/ProteinSimple, USA).

Quantitative real time RT-PCR (qRT-PCR) was performed using the Absolute qPCR SYBR Green Fluorescein Mix (AB-1219, Thermo Scientific) according to manufacturer's protocol. Reference genes were CD31 (vessels fragments analysis) or Rplp0. Expression data were analysed (CFX96, Biorad) and significance was calculated with GraphPad Prism 6.0 software using a *t*-test for all analyses except for the TEER experiments for which a one-way ANOVA followed by a Tukey's multiple comparison test was applied. Primer sequences used for cDNA amplification by qRT-PCR are listed in Table 2.

2.5. Immunohistochemical staining and quantification on cryosections and MBMVs

Post anaesthesia, mice were i.v. injected with tomato lectin-Alexa 649, and was allowed to circulate for 5 min before sacrificing the animal. Mice were sacrificed by cervical dislocation and brains were collected and frozen in native state in O.C.T. and stored at −80 °C. Coronal sections (10 µm, from bregma 0.98 and -1.82 mm) were fixed in ice-cold MetOH for 3 min followed by 1 h incubation in

Table 2
Primer sequences used for cDNA amplification by qRT-PCR.

Primer for	Sequence 5′-3′ sense	Sequence 5′-3′ antisense
qmm_Abcb1a/P-gp	gctatcacggccaacatctcc	tgtccaacactgaatgctccaa
qmm_Abcg2	tggcatctctggaggagaaaga	cgaggctgatgaatggagaaga
qmm_Axin2	gccgacctcaagtgcaaactc	ggctggtgcaaagacatagcc
qmm_Cav1	gacgcgcacaccaaggagatt	ctgaccgggttggttttgat
qmm_CD31	attcctcaggctcgggtcttc	ccgccttctgtcacctccttt
qmm_Cdh5/VE-cadherin	gcccagccctacgaacctaaa	gggtgaagttgctgtcctcgt
qmm_Cldn5	tgtcgtgcgtggtgcagagt	tgctacccgtgccttaactgg
qmm_Ctnnb1/β-catenin	gagcacatcaggacacccaac	gttgtgaacgtcccgagcaag
qmm_Evi/Wls	ccgtgacatggaggaagcaa	ggtaacccagggaaacatcca
qmm_Fzd1	tgtcccttgcccagtgtcttt	tttagcctctcccaacccaca
qmm_Fzd2	cccgacggctctatgttcttc	cgcaatgtaggccactgacac
qmm_Fzd3	cgtggcctgaagatatggagtg	cgtgcagaaaggaatagccaag
qmm_Fzd4	tcggctacaacgtgaccaaga	tggcacataaaccgaacaaagg
qmm_Fzd5	ctcttctgctgctgttgctgg	ggcatgtgcgtcaggttgtag
qmm_Fzd6	tcacctgggagatgacatggtt	caacccagaagaccgcagaga
qmm_Fzd7	ctacctgggctaccgcttcct	cagcacagcactgaccacaca
qmm_Gpr124	caccatcaccttgctcttgagc	agattgctcctcaggtccaact
qmm_Ndp	gccaatgtgacagagggacag	caaggccagagcaggatagg
qmm_Tspan12	acaagggtagaagaagcggtca	accgttccacagtatcccagca
qmm_Wnt4	ggcgtagccttctcacagtcc	acgccagcacgtctttacctc
qmm_Wnt5a	tctccttcgcccaggttgtt	cctgtcttcgcaccttctcca
qmm_Wnt5b	gctgctgactgacgccaact	gcactctctgatgcccgtctt
qmm_Wnt6	gaggctgcggagacgatgtg	agagcgcaggaacccgaaag
qmm_Wnt7a	cgccaaggtcttcgtggatg	cggcctcgttgtatttgtcct
qmm_Wnt7b	tttctcgtcgctttgtggatg	gcctgacacaccgtgacactt
qmm_Wnt9a	gccagtaccagttccgctttg	cggcagaagagatggcgtaga

permeabilization-saturation buffer (5% BSA in PBS with 0.1% Triton). Primary antibodies (for detail see table Table 1) were incubated overnight at 4 °C in 0.5% BSA in PBS 0.1% Triton, and secondary antibodies for 2 h at RT. Following nuclear staining with DAPI, slides were mounted with Fluoromount-G (#00−4958-02, Invitrogen, Germany).

Vessel fragment staining started after fixation in 4% paraformaldehyde (PFA) with subsequent quick PBS washes and permeabilization-saturation as presented above. Mouse anti-desmin, rat anti-CD31 and rabbit anti-AQP4 dilutions are presented in Table 1. Images were acquired using a Nikon C1si or Nikon A1RHD25 Confocal Laser Scanning Microscope Systems, together with NIS Elements Microscope Imaging Software (Nikon Instruments, Inc., Düsseldorf, Germany).

To assess junction protein localization and expression, images were taken with the 60x objective with a 1.5x electronic zoom from 3 animals of each age and genotype. Two independent researchers evaluated the blinded images with the scoring system depicted in Fig. S5A.

2.6. Immunohistochemical staining and quantification on vibratome sections

For quantitative analysis of vasculature network, pericyte and astrocyte coverage as well as neuronal activation, mice were anesthetized and then transcardially perfused with PBS for 2−3 min to remove blood from vessels. The brains were dissected and post-fixed overnight in 4% PFA. Serial 50 µm coronal sections were cut on a VT 1000S Leica Vibratome (Leica Biosystems GmbH, Germany). In order to detect endothelial cells, pericytes, astrocyte endfeet and activated neurons, rat anti-CD31 (if not injected with tomato lectin), goat anti-CD13, rabbit anti-Aqp4 and rabbit anti-c-fos antibodies were used, respectively. Free-floating sections were incubated for 1 h in permeabilization-saturation buffer (5% BSA in PBS with 0.1% Triton) before a 48 h incubation with primary antibodies at 4 °C in 0.5% BSA in PBS 0.1% Triton buffer. After PBS washes, secondary antibodies were incubated for 2 h at RT or overnight at 4 °C. Following nuclear staining with DAPI, free-floating sections were mounted on slides with Fluoromount-G.

Sections from different bregma levels (0.98 and -1.82 mm, Fig S3) were analysed and 30 µm confocal stacks from several area were taken with a Nikon C1si or A1RHD25 Confocal Laser Scanning Microscope System, using NIS Elements Microscope Imaging Software (Nikon Instruments, Inc., Düsseldorf, Germany).

Vascular area and branching point analyses were performed on maximum intensity projection of the 30 µm confocal stacks on NIS Elements Microscope Imaging software (Nikon). For pericyte volume and astrocyte endfeet coverage analyses, a threshold was set to create a binary mask of CD13 and AQP4 stainings on each z step of the 30 µm confocal stack. Thereafter, the generated binary surface and the known z step size were used to calculate the volume of the staining by the NIS Elements Microscope Imaging software (Nikon). These values were normalized to the vessel volume determined accordingly for the CD31 staining. Significance was calculated with GraphPad Prism 6.0 software using a *t*-test. Volume/surface rendering of the Aqp4 staining was created with Imaris 9.0 software (Bitplane, Switzerland).

2.7. Electron microscopy

Animals were anesthetized and transcardially perfused with PBS for 1 min followed by 4 min with 4% PFA in PBS. The isolated brains were post-fixed in 4% PFA and 2% glutaraldehyde in PBS overnight at 4 °C. The tissue was cut into small pieces and additionally post-fixed in the same fixative overnight, followed by incubation in 1% OsO4 for 2 h at RT with subsequent staining with lead citrate solution and 2% uranyl acetate solution at 4 °C overnight prior to embedding. After dehydration in a graded acetone series, the final polymerization in Durcupan was performed at 60 °C for 72 h. Sections were analysed using a Tecnai Spirit BioTWIN FEI electron microscope at 120 kV. Images were acquired with an Eagle 4 K CCD bottom-mount camera. For the quantification of vesicles, 12–19 cortical vessels of comparable size (4 µm diameter) were analysed for each animal (n = 3 per genotype). The total vesicles counts were normalized to the endothelial cytoplasm area and the abluminal and luminal vesicles were normalized to the length of their respective membrane side as depicted in Fig. 6B. Significance was calculated with GraphPad Prism 6.0 software using a *t*-test.

2.8. Massive analysis of cDNA ends (MACE)

2.8.1. Cell isolation and FACS sorting

Brains of adult mice were collected individually, and subsequently olfactory bulbs, cerebellum, hindbrain and choroid plexus were removed, and forbrains were rolled on sterile Whatman paper to remove meninges. Two brains from the same genotype were pooled and immediately stored on ice in buffer A (Czupalla et al., 2014). They were subsequently homogenized in the same buffer using a dounce homogenizer and centrifuged at 400 *g* for 10 min at 4 °C. Following myelin removal by 25% BSA centrifugation as described in MBMV isolation, the pellet was resuspended in buffer A and cells were filtered through a 70 µm mesh to remove the bigger undigested vessels or tissue clamps. The suspension containing isolated cells and small vessels fragments was digested again with Collagenase/Dispase (#10269638001, Roche) and DNase I (#LS006333, Worthington) solution for 15 min at 37 °C, under gentle agitation. After Red blood cell lysis (#11814389001, Roche), cell suspension was stained with anti-CD31 antibody conjugated to PE-Cy7 (#25−0311-81, clone 390, Biolegend) diluted 1:100 in FACS buffer (5% serum in PBS). Before sorting, DAPI was added for live cell gating and cells were sorted and collected directly in RLTplus buffer using a FACSAria flow cytometer equipped with Diva Software (BD Bioscience, Germany). RLTplus samples were stored at −80 °C until RNA isolation was performed according to manufacturer's recommendation.

2.8.2. Transcriptome profiling by MACE-Seq

Preparation and next-generation sequencing of MACE-Seq libraries was performed using the "MACE-Seq kit v2.0″ (GenXPro GmbH, Frankfurt, Germany) according to the supplier's manual.

In general the procedure follows a modified protocol described in Nold-Petry et al. (Nold-Petry et al., 2015). In short, 15 ng of DNase treated RNA per sample were used for library preparation. cDNA was produced by oligo dT priming and then was sheared to an average size of 200 bp. Fragments were ligated to "TrueQuant" unique molecular identifiers included in the kit. MACE-Seq tags were amplified with 13 PCR cycles and the libraries were sequenced on an Illumina NextSeq 500 sequencer.

2.8.3. Bioinformatics analysis of MACE-Seq data

A total of ~28 million MACE-Seq sequencing reads were obtained from the two cDNA sequencing libraries. All PCR duplicated reads identified by the TrueQuant technology were excluded from the raw data sets. The remaining reads were further qualitatively trimmed, and the poly (A)-tail was clipped off. Filtered reads were aligned to the *Mus musculus* reference genome (GRCm38.p5) using the bowtie2 mapping tool (Langmead and Salzberg, 2012). The GRCm38.p5 Ensembl annotation GTF file was imported into the htseq-count annotation tool to annotate bam files. Next, normalization of gene count data followed by differential gene expression analysis between the samples was performed using the DEGseq R/Bioconductor package (Wang et al., 2019). The following thresholds were chosen for significantly differentially expressed genes: raw expression $\geq$ 20 reads, $0.5 \leq \log_2$fold change ≥ -0.5, p-value ≤ 0.05. Gene Ontology enrichment analysis was performed using g:Profiler (https://biit.cs.ut.ee/gprofiler/gost). Volcano plots were created using GraphPad Prism software, while visualization of most relevant GO classes was performed using GOPlot library (R, Bioconductor, (Walter et al., 2015)).

2.9. Primary cell isolation and culture

Primary astrocytes were isolated as described by Uliasz et al. from pups aged between 2 and 4 days and were cultured on poly-L-lysine coated cell culture plates in DMEM-Glutamax medium containing 10% FCS and 1% penicillin-streptomycin (Uliasz et al., 2012).

A modified protocol was utilized to isolate endothelial cells for *in vitro* cell culture experiments (Liebner et al., 2008; Paganetti et al., 2014). Briefly, meninges-free brains from adult mice were pooled and homogenized as described above followed by digesting the pellet with collagenase II (0.75%, C2−28, Biochrom) in buffer A (1:1:1 vol ratio) for 1 h with shaking at 37 °C. For the removal of myelin, samples were resuspended in 25% BSA/PBS and centrifuged at 2000 *g* for 20 min at 4 °C followed by enzymatic digestion of the pellet with Collagenase/Dispase (#10269638001, Roche) and DNase I (#LS006333, Worthington) in buffer A for 15 min at 37 °C. After centrifugation, cells were resuspended in MCDB-131 complete medium according to Czupalla et al. (Czupalla et al., 2014) with slight modifications (MCDB-131-based growth medium containing 20% FCS, 2 mM L-glutamine, 1% penicillin-streptomycin, 1% homemade ECGS, 5 mM heparin, 1 mM sodium bicarbonate), and seeded on six-well plates pre-coated with type 1 collagen (150 μg/cm^2, #344236, Corning). After 6 h, the medium was changed to puromycin-containing medium (4 μg/mL, #P9620, Sigma-Aldrich) to select for brain ECs (Devraj et al., 2016; Liebner et al., 2008). After 2 days, the medium was changed back to puromycin-free medium. Following passages were cultured in the same medium if not specified otherwise but with fibronectin coating of the plates/inserts (1:100 dilution, #F1141, Sigma-Aldrich). Porcine brain microvascular endothelial cells (PBMEC) were isolated and cultivated the same way except that the collagenase II stock solution was 0.25%.

For Wnt3a treatment, primary mouse brain microvascular ECs (MBMECs) were seeded on 24 well plates (2.5*10^4 cells/cm^2) in complete MCDB-131, containing 150 ng/mL mouse recombinant Wnt3a (#315−20, Peprotech) or 0.1% BSA as a control. After 3, 6 and 9 days of culture, with the medium replaced every 3 days, the cells were washed twice with cold PBS, and collected in RLTplus lysis buffer for RNA analysis. For GSK3β inhibition treatment PBMECs were seeded on 6 wells plates and upon confluency were treated for 24 h with 2.5μM Bio-X or DMSO (0.15%) as control. At the end of the treatment, cells were washed several times with ice-cold PBS and collected in urea/SDS solubilization buffer (2.3 M urea, 1.5% SDS, 50 mM Tris, 25 mM TCEP and 0.01% BPB; 1.5 h at 30 °C) for further protein analysis.

2.10. Impedance measurement

Transendothelial electrical resistance (TEER) and capacitance (Ccl) measurements were performed in a cellZscope® device (nanoAnalytics, Münster, Germany) with MBMECs (10^{5}cells/cm^2) seeded on the top of 24-well filter inserts (PET ThinCerts™, 1.0 μm pore size, 2 × 10^6 pore density, Greiner Bio One, Germany) in presence or absence of primary astrocytes seeded on the bottom part of the same insert. Analysis of TEER and Ccl data was monitored and recorded until values reached a plateau phase (36–72 h). Each experimental condition within a set, consisting of the same preparation of MBMECs and the respective coculture with primary ACs from Evi$^{\Delta AC}$ and Evi^{Ctrl} pups, were carried out in quadruplicates (n = 4) in MBMECs culture medium. Data was monitored and analysed in the provided cellZscope® software (version 1.5.3). For further information see also Paolinelli et al. (Czupalla et al., 2014; Paolinelli et al., 2013). Significance was calculated with GraphPad Prism 6.0 software using a 2way ANOVA with a Sidak's multiple comparison test. At the end of the experiment, inserts were either used for *in vitro* permeability assays, for RNA isolation (2 inserts pooled) or fixed with ice-cold methanol (3 min) for staining as described in detail in Czupalla et al. (Czupalla et al., 2014).

2.11. In vitro permeability assay

Fluorescently labelled tracers 0.45 kD Lucifer yellow (LY, #L0144, Sigma-Aldrich), 3 kD Texas Red® Dextran (TXR 3 kD, #D3328, Thermofischer), 20 kD tetramethylrhodamine isothiocyanate dextran (TMR 20 kD, #73766, Sigma-Aldrich) in a final concentration of 10 μM and 70 kD Fluorescein isothiocyanate dextran (FITC 70 kD, 5μM, #FD70S, Sigma-Aldrich) were added to the top chamber of the filter inserts previously used for impedance measurement. Samples were taken from the bottom chamber after 1 and 3 h of incubation at 37 °C. Fluorescence was analysed using the following order of excitation/emission (nm): TXR 595/625, TMR 550/580, FITC 490/520, LY 425/525. Permeability flux was calculated as a ratio of bottom to top chamber fluorescence (R = B/T) (Czupalla et al., 2014). Co-culture with AC KO for Evi results are expressed as percentage of the paired co-culture with AC control. At least 3 inserts per condition were used for each experimental set. Significance was calculated with GraphPad Prism 6.0 software using a 2way ANOVA with a Sidak's multiple comparison test.

2.12. Immunofluorescence on MBMECs co-culture with astrocytes

Staining procedure was the same as described above for cryosections. Mouse anti-Cldn5, rabbit anti-Cav-1, goat anti-Cdh5 and corresponding secondary antibodies were used according to the dilution in Table 2. Images were taken with a Nikon C1si confocal microscope and were processed and analysed with NIS Elements AR Imaging Software (Nikon, Düsseldorf, Germany).

2.13. Western Blot analysis

MBMEC, PBMEC or MBMV samples in HES buffer were thawed, sonicated and solubilized in SB buffer (2.3 M urea, 1.5% SDS, 15 mM Tris, 500 mM TCEP and 0.01% BPB) for 1 h at 30 °C. Electrophoresis and transfer were performed by standard submerged method followed by western blotting. Primary and secondary antibodies were diluted in Roti-block (#A151, Roth) and incubated overnight at 4 °C and 1 h at RT, respectively (for reference detail see Table 3). Blots were visualized utilizing an Odyssey FC digital imaging system (LI−COR Biosciences) and quantitation was performed using Image Studio software (version 2.1.10). Protein levels were normalized to β-actin/Actb.

2.14. Statistical analysis

Results are shown as mean ± SEM. Statistical significance was calculated with Prism version 6.0; GraphPad Software. Statistical analysis was performed as indicated in each material and method section. P-values <0.05 were considered significant (**** <00.001; *** 0.001 to 0.001; ** 0.001 to 0.01; * 0.01 to 0.05).

Table 3
Antibodies for western blot analysis.

Antibody	Company	Catalog #	Dilution
Abcb1a/Pgp (C219)	Thermo Fisher	MA1−26528	1:500
Actb	Santa Cruz	sc99879	1:1000
Caveolin-1	BD Transduction	610,057	1:1000
Cdh5/VE-Cadherin	Santa Cruz	sc6458	1:500
Cldn5	Thermo Fisher	34−1600	1:200
Slc2a1/Glut1	Rabbit C-ter, see (Devraj et al., 2011)		1:2000
Goat α-rabbit 800	LI-COR	926−32211	1:2000
Goat α-mouse 680	LI-COR	926−68070	1:2000
Donkey α-mouse IgM 650	Thermo Fisher	SA5−10153	1/2000
Donkey α-mouse IgG 680	LI-COR	926−68072	1/2000
Donkey α-goat 800	LI-COR	926−32214	1/2000

3. Results

3.1. Evi$^{\Delta AC}$ mice are viable and show mild brain oedema and BBB impairment

In order to understand if AC-derived Wnt growth factors may contribute to the maintenance of endothelial BBB characteristics at the NVU, we initially tested and confirmed the expression of Wnt family members in freshly isolated and passaged ACs *in vitro* (Fig. S1). As expected, several Wnt ligands were detected including Wnt7a and Wnt7b that are known to be crucial for developmental brain angiogenesis and barrier formation (Fig. S1A, F). Moreover, ACs express the non-canonical Wnt ligands Wnt4, Wnt5a and Wnt11. In comparison to ECs, ACs express higher amounts of most of the Wnt genes tested by qPCR with exception of Wnt6 (Fig. S1F). Astrocytes also express several frizzled (Fzd) receptors, Lrp5/6 as well as Wnt inhibitors from the soluble frizzled-related proteins (Sfrp) family (Fig. S1B-D, G). In addition to the expression of Wnt growth factors, receptors and other Wnt pathway-related genes, ACs express the non-Wnt-related Fzd ligand Ndp that can activate β-catenin transcriptional activity *via* an alternative receptor complex including Gpr124 and Tspan12 (Fig. S1H).

To achieve constitutive, genetic ablation of Evi specifically in ACs we crossed the hGFAP-Cre (Bajenaru et al., 2002) with the Evi$^{flox/flox}$ mouse line (Carpenter et al., 2010). Global AC-specific Cre activity and recombination was confirmed by crossing the hGFAP-Cre to the ROSA26-mTmG reporter line (Muzumdar et al., 2007), suggesting a homogeneous recombination throughout the CNS (Fig. S2A). Although we could not directly detect recombination by staining for Evi due to the lack of suitable antibodies, we confirmed the astrocytic recombination in the Evi$^{\Delta AC}$ CNS tissue by the co-localization of GFAP (astrocyte intracellular protein) with β-galactosidase, which is expressed in parallel to the Cre-recombinase downstream of an IRES site (Fig. S2B) (Bajenaru et al., 2002).

Cre-expressing, Evi$^{flox/flox}$ homozygous mice (Evi$^{\Delta AC}$) were born in the expected Mendelian ratio (Fig. 1A), were viable and did not show any gross morphological and behavioural deficits (data not shown). Nevertheless, Evi expression in freshly isolated ACs was diminished by roughly 90%, suggesting successful deletion in the majority of ACs (Fig. 1B). In order to understand if the vascular system, and the NVU in particular, is morphologically and functionally affected by astrocytic deletion of Evi, we firstly analysed vascular density (measured as vascular area fraction in thick sections) and branching in young and middle-aged adults of 10 and 40 weeks, respectively (Fig. S3). This analysis was carried out for different brain regions such as the cortex, subcortical regions, hippocampus, thalamus and others (see Fig. S3I, J), to be able to determine effects related to specific brain areas. We did not observe an altered vascularized area fraction between Evi$^{\Delta AC}$ and Evi^{Ctrl} mice neither at 10 weeks, nor at 40 weeks of age (Fig. S3A, C, E, G). Along this line, we also analysed vascular branching, which did not show significant differences at both ages (Fig. S3B, D, F, H). This suggests that the ablation of astrocytic Wnt growth factor release does not affect postnatal angiogenesis and vascular remodelling, resulting in a normal vascular network in the adult.

To investigate the functional integrity of the BBB, we firstly characterized the water content in the tissue, as a surrogate marker for brain oedema. Brain mass from mature adult (10–20 weeks) Evi$^{\Delta AC}$ and Evi^{Ctrl} mice was measured before and after drying of the tissue to calculate the wet/dry weight ratio. The brain weight/body weight (%) of the wet mass of the brains did not significantly differ (Fig. 1C). Comparison of the entire brain, including cortex, subcortical areas, cerebellum and hindbrain revealed a significant increase in water content in the Evi$^{\Delta AC}$ mice (Fig. 1D). By separating the cortex and subcortical regions from the cerebellum and hindbrain in this analysis, it turned out that increased water content was restricted to the cortex/subcortical regions, whereas the cerebellum/hindbrain did not significantly differ (Fig. 1E, F). We did not observe differences between male and female mice regarding the water content (data not shown). *In vivo* permeability assays confirmed this finding in the spinal cord and cortex for the small molecular tracer fluorescein-5-thiosemicarbazide (FTSC, 0.42 kDa), whereas for the slightly bigger tracer TMR-dextran (3 kDa) also the cerebellum showed a significantly higher extravasation in the Evi$^{\Delta AC}$ mice (Fig. 1G, H, I). As expected, organs harbouring leaky blood vessels like the kidneys or the liver, which served as a positive control, did not reveal any differences in extravasation between Evi^{Ctrl} and Evi$^{\Delta AC}$ mice (Fig. 1 H, I and not shown). In addition to the quantitative analysis of the total extravasated tracer in the supernatant of the homogenized brain, we qualitatively analysed tracer extravasation *via* IF microscopy upon intravenously injected Alexa Fluor® 555 Cadaverine (~1 kDa; A555-Cad), which was allowed to circulate for 5 min prior to sacrification of the animal. Qualitative analysis revealed increased leakage of A555-Cad in Evi$^{\Delta AC}$ mice compared to Evi^{Ctrl} mice at 10- (data not shown) and 40-weeks of age, evidenced by the accumulation of the tracer in cortical neurons (Fig. 1J).

3.2. Wnt and BBB-related genes are downregulated in brain vessels of Evi$^{\Delta AC}$ mice

Next, we wanted to understand if the Wnt pathway, as well as BBB-related genes, were affected by Evi ablation in ACs at the NVU. To this end, we harvested mouse brain microvessels (MBMVs) from young adult (10 weeks) as well as from middle-aged adult (40 w) mice, isolated the RNA and analysed gene expression by quantitative real-time PCR (qRT-PCR). It should be noted that the isolated MBMVs contain ECs, PCs and AC end-feet that is documented by the staining for CD31, desmin and aquaporin-4 (Aqp4), respectively (Fig. 2A right panel). The Wnt/β-catenin target gene Axin2, as well as Ndp were not differentially expressed in MBMVs of 10-week-old Evi$^{\Delta AC}$ mice, whereas the Wnt/β-catenin target Nkd1, a negative feedback regulator of the pathway, was significantly downregulated (Fig. 2B left panel). In MBMVs of 40-week-old Evi$^{\Delta AC}$ mice both Axin2 and Nkd1 turned out to be significantly downregulated, suggesting that β-catenin signalling is persistently and substantially affected at the NVU (Fig. 2B right panel). Given the significant increase in water content and tracer permeability of Evi$^{\Delta AC}$ mice, we further analysed the expression of junctional genes by qRT-PCR. Although we observed a trend for downregulation of several junctional genes like Cdh5/VE-Cadherin, Cldn5, Occln and Tjp1/ZO-1 in 10-week-old Evi$^{\Delta AC}$ mice, none of them were significantly reduced on the mRNA level (Fig. 2C left panel). Interestingly, Ctnnb1 expression did not present any alteration between the conditions in 10-week-old mice (Fig. 2C left panel). The general lower expression of junction genes in Evi$^{\Delta AC}$ mice was also true for 40-week-old mice, showing a significant downregulation of Cdh5 and Tjp1 (Fig. 2C right panel). The downregulation of Cdh5 could also be confirmed by western blot analysis, showing a reduced protein expression by densitometric analysis in lysates from MBMVs of 10-week-old Evi$^{\Delta AC}$ compared to Evi^{Ctrl} mice (Fig. S4). Cldn5 showed in trend a downregulation also on the protein level, which however was not significant (Fig. S4).

To investigate the distribution and localization of junctional proteins at the BBB, we specifically evaluated Cdh5 and Cldn5 by immunofluorescence staining and site-directed analysis of junctional organization of these proteins in 10- and 40-week-old mice. The detailed quantitative analysis of staining showed no obvious differences for the two junction molecules with regard to intensity, continuity and pattern in cortical vessels, as well as in other regions of the brain (Fig. 3A, B, Fig. S5). Moreover, electron microscopy analysis revealed that Evi$^{\Delta AC}$ mice show now obvious structural alterations of cortical, inter-endothelial junctions (Fig. 3C).

The expression of BBB-associated transporters like Abcb1a/P-gp, Abcg2, and Slc2a1/Glut1, was not significantly regulated in MBMVs at both time points analysed (Fig. 2D). Glut1 did not show a differential expression or distribution in immunofluorescent staining (Fig. S4 C).

Given that for vascular and BBB integrity the extracellular matrix

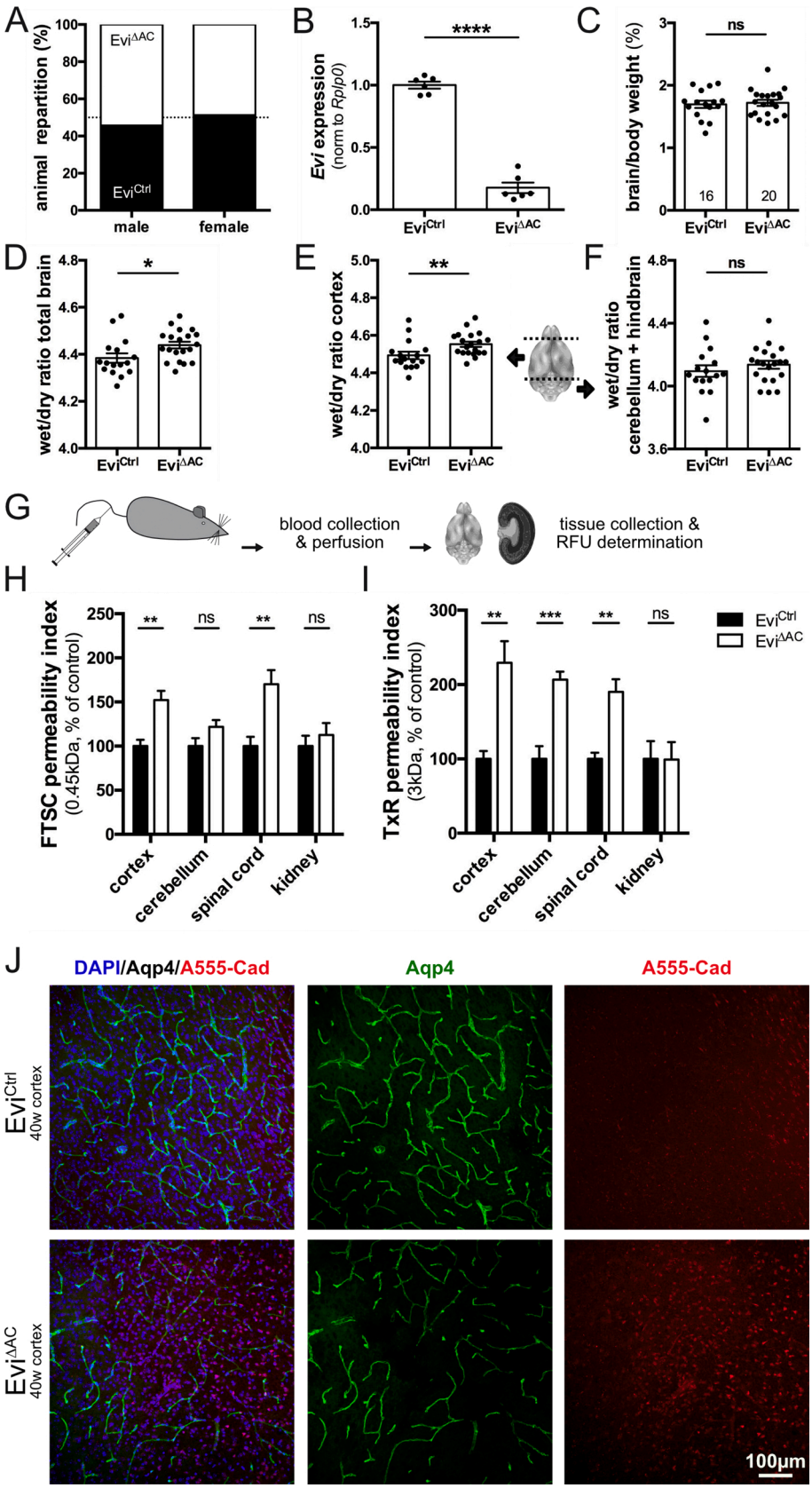

Fig. 1. Evi deletion in astrocytes induces mild oedema and alters BBB permeability.
(A) Constitutive deletion of Evi in ACs follows a mendelian repartition (n = 284♂, 302♀). (B) Evi expression is reduced by 90% in cultivated ACs (passage 1) isolated form P3−5 pups (n = 6). (C) Analysis of the brain/body ratio of $Evi^{\Delta AC}$ animals compared to Evi^{Ctrl} (n = 20 and 16 respectively). (D) Analysis of the wet/dry weight ratio in the total brain of $Evi^{\Delta AC}$ mice. (E) wet/dry weight ratio for cortex, (F) and the cerebellum + hindbrain. (G) Scheme of *in vivo* tracer permeability assay. (H, I) Quantitative analysis of extravasated FTSC 0.45 kDa and Texas Red 3 kD tracers upon intravenous injection by fluorescence measurement of brain homogenate supernatants from 10-20-week-old mice (n = 5–6). (J) Qualitative microscopic analysis of Alexa555-cadaverin extravasation in 50 µm vibratome brain sections of 40-week-old mice (representative images of n = 3).

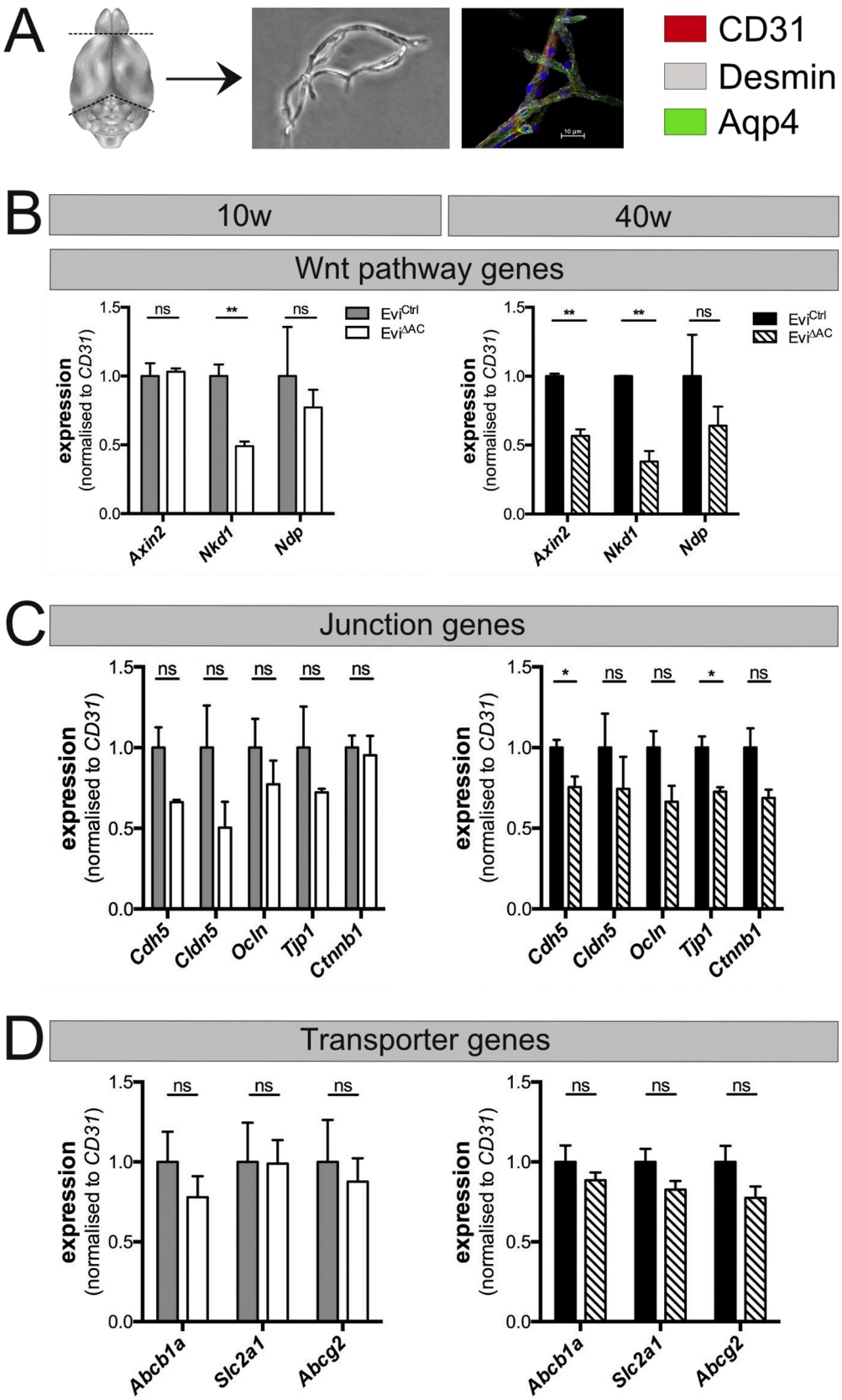

Fig. 2. Wnt targets and some junction genes are down regulated in vessels fragments from Evi$^{\Delta AC}$ animals at different age. (A) Vessel fragments were isolated from the cerebrum part of the brain of 10- and 40-week-old mice and subjected to qRT-PCR analysis. It has to be noted that these fragments contain EC, PC and AC end-feet as shown by CD31, Desmin and AQP4 staining on the right panel. (B) Analysis of the Wnt pathway genes *Axin2*, *Nkd1* and *Ndp*. (C) Analysis of junctional genes *Cdh5*, *Cldn5*, *Occl*, *Tjp1* and *Ctnnb1*. (D) Analysis of the transporter genes *Abcb1a*, *Slc2a1* and *Abcg2*. For each age and genotype n = 3 mice.

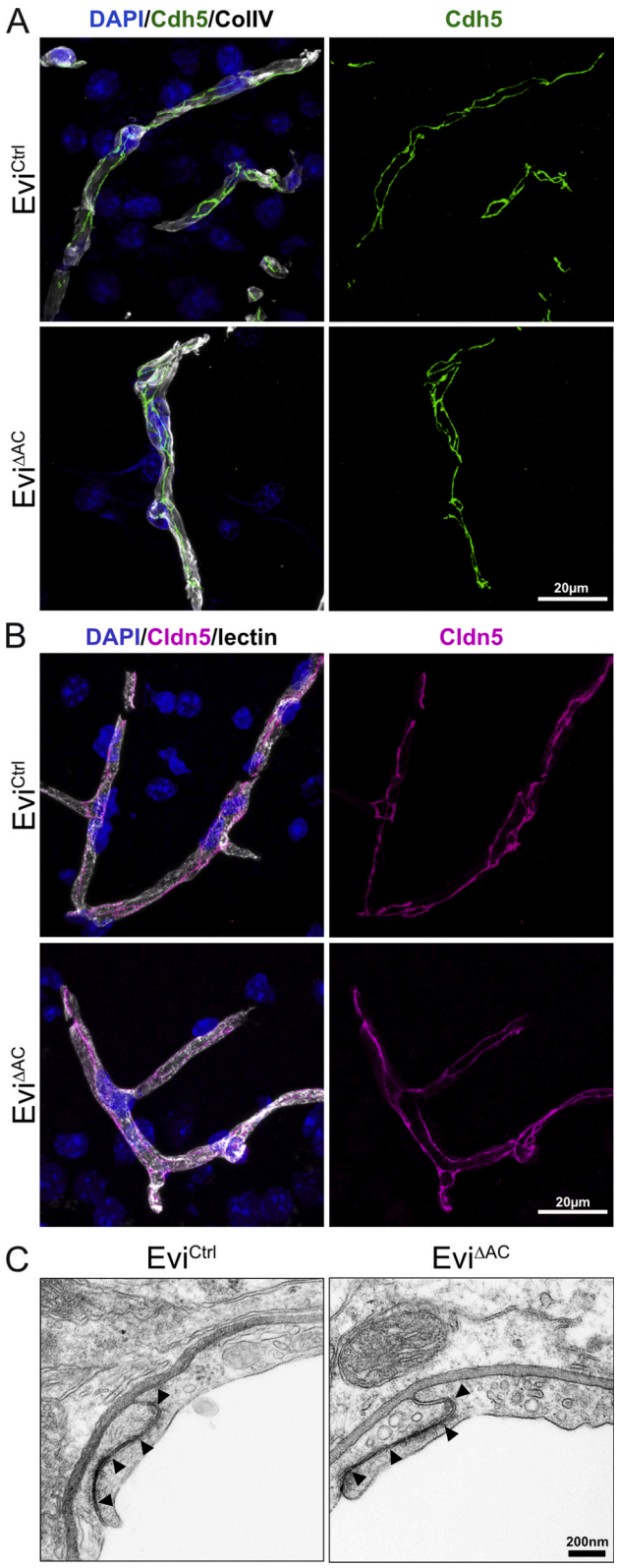

Fig. 3. Junction markers do not seem affected in Evi$^{\Delta AC}$ animals.
(A–B) Immunohistochemistry on 10 µm cryosections of cortex tissue from 40-week-old mice for Cdh5 (A, green) collagen IV (white) as vessel marker, and Cldn5 (B, magenta) with tomato lectin (white) as vessel marker. (C) Transmission electron microscopy of tight junctions between cortical brain endothelial cells from both Evi^{Ctrl} and Evi$^{\Delta AC}$ animals. Representative picture of n = 3.

composition of the basement membrane (BM) plays a crucial role, we have stained for collagen IV (Fig. 3A), laminin α2 (Lama2; parenchymal, astrocytic BM), laminin α4 (Lama4; vascular constitutive) and laminin α5 (Lama5; vascular differentially regulated) (Fig. S6). However, we could not identify differences in expression and/or localization of these BM markers in 10- and 40-week-old mice.

3.3. Cortical endothelial cells of Evi$^{\Delta AC}$ mice exhibit an "activated" phenotype evidenced by RNA-Seq analysis

In order to investigate the effects of astrocytic Evi deletion on cortical ECs in an unbiased fashion, we performed next generation sequencing by 3′-poly A tail based Massive Analysis of cDNA Ends (MACE) of RNA isolated form ECs that were FACS-sorted against CD31 from young adult mice (Fig. S7A, B). A total of 8103 annotated RNAs were expressed, of which 958 were up and 236 were down regulated between Evi^{Ctrl} and Evi$^{\Delta AC}$ cortical ECs with more than 20 raw reads per annotated gene and log2FC higher than 0.5 in absolute value. In order to qualitatively evaluate the cellular identity of the RNA subjected for MACE analysis, we analysed the reads for marker genes of the NVU according to commonly used markers and the cell specific gene expression identified by single cell RNA-Seq by Vanlandewijck as well as Zhang and colleagues (Vanlandewijck et al., 2018; Zhang et al., 2014). We could only detect minimal contamination by ACs and PCs that are anatomically closely attached cell types at the NVU (Fig. 4A). Gene ontology (GO) enrichment analysis revealed that the canonical Wnt pathway was significantly regulated, whereas the non-canonical Wnt pathway did not show a significant regulation in isolated brain EC from Evi$^{\Delta AC}$, suggesting that Evi deletion in ACs predominantly affects canonical Wnt growth factors acting on the vascular endothelium (Fig. 4B, C, D). Moreover, the establishment of the endothelial barrier GO term was significantly upregulated in Evi$^{\Delta AC}$ cortical ECs (Fig. 4E). Interestingly, we could not confirm the downregulation of junctional genes. Surprisingly, Cdh5 showed a slight but significant upregulation in the RNA-Seq data set, whereas Cldn5 was not regulated. In line with the GO regulation for barrier establishment, GOs for vascular development, adherens junctions (Fig. S7C), endothelial cell differentiation (Fig. S7G), extracellular matrix (Fig. S7H) as well as for caveolae (Fig. 4F) showed a significant regulation, suggesting that cortical ECs in Evi$^{\Delta AC}$ mice are in an "activated state" (Fig. S7).

Notably, caveolin-1 (Cav-1), as well as Cav-2, which are part of the canonical Wnt pathway and crucial components of the caveolae machinery, were upregulated in cortical ECs of Evi$^{\Delta AC}$ mice. This may suggest an increased transcytotic activity in Evi$^{\Delta AC}$ animals.

3.4. Astrocytes from Evi$^{\Delta AC}$ mice support high resistance in TEER measurements but promote transcellular permeability of tracers in a BBB co-culture model in vitro

In order to test the hypothesis of increased endothelial transcytosis and to further investigate the junctional contribution to vessel permeability in Evi$^{\Delta AC}$ mice, we made use of a well-established *in vitro* co-culture model, in which ACs have been proven to promote endothelial barrier function (Haseloff et al., 2005). In order to understand if Wnt growth factors derived from ACs play a role in this *in vitro* co-culture paradigm of the BBB, we isolated ACs from Evi^{Ctrl} and Evi$^{\Delta AC}$ pups and subjected them at passage 1 (P1) to co-culture with primary mouse brain microvascular endothelial cells (MBMECs) on transwell® filters (Fig. 5A). The Trans Endothelial Electrical Resistance (TEER) as well as the capacitance (Ccl) were continuously measured using the cellZscope® device. We could confirm previous reports that control ACs lead to increased and stabilized TEER values in MBMECs compared to mono-cultures (Fig. 5B). Conversely, Ccl values were considerably lower in the co-culture with control ACs compared to the MBMEC alone (Fig. 5C). This corresponds to a tighter alignment and better flattening of ECs, which are characteristics of the brain endothelium. Surprisingly,

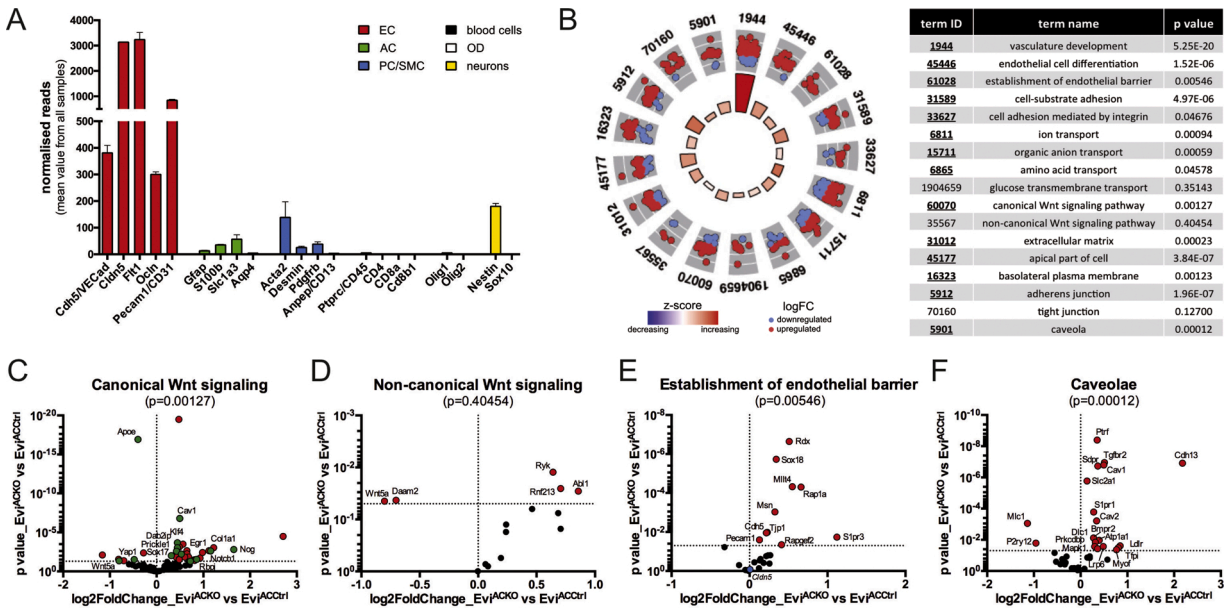

term ID	term name	p value
1944	vasculature development	5.25E-20
45446	endothelial cell differentiation	1.52E-06
61028	establishment of endothelial barrier	0.00546
31589	cell-substrate adhesion	4.97E-06
33627	cell adhesion mediated by integrin	0.04676
6811	ion transport	0.00094
15711	organic anion transport	0.00059
6865	amino acid transport	0.04578
1904659	glucose transmembrane transport	0.35143
60070	canonical Wnt signaling pathway	0.00127
35567	non-canonical Wnt signaling pathway	0.40454
31012	extracellular matrix	0.00023
45177	apical part of cell	3.84E-07
16323	basolateral plasma membrane	0.00123
5912	adherens junction	1.96E-07
70160	tight junction	0.12700
5901	caveola	0.00012

Fig. 4. MACE analysis on FACS isolated ECs.
(A) Mean reads for markers of EC, AC, PC, blood cells, oligodendrocytes and neurons confirm the low contamination of other cell types in the isolated brain ECs (from 2 young animals pooled for each genotype). (B) GO Circle plot for BBB- and Wnt-relevant GO terms, representing up or down regulated genes in Evi$^{\Delta AC}$ brain ECs compared to Evi^{Ctrl}. (C–F) Volcano plots of single GO term including genes belonging to (C) Wnt canonical pathway, (D) Wnt non-canonical pathway, (E) establishment of endothelial barrier (F) and caveolae groups. Red dots represent significantly regulated genes, green dots indicate significantly regulated genes belonging to both Wnt canonical pathway and vascular development and blue dots highlight unregulated genes investigated in this study.

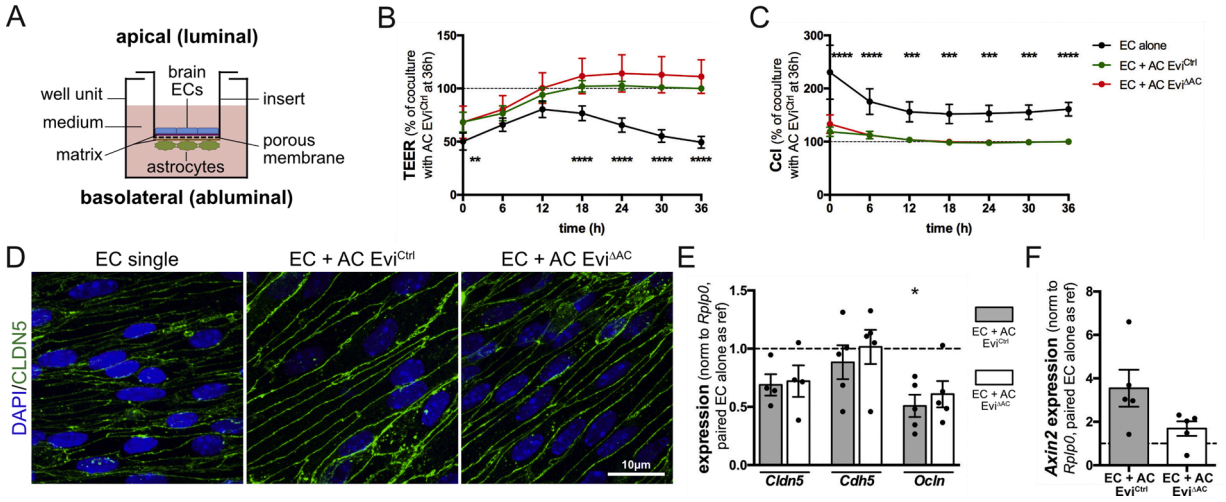

Fig. 5. Transendothelial electrical resistance and capacitance of brain ECs is not affected by coculture with ACs from Evi$^{\Delta AC}$.
(A) Schematic of the *in vitro* BBB model using co-culture of ACs and MBMECs in direct contact *via* a porous membrane. (B) Transendothelial electrical resistance (TEER) and (C) capacitance (Ccl) of the endothelial monolayer in mono-culture and co-culture with ACs from Evi^{Ctrl} or Evi$^{\Delta AC}$ mice (n = 4). (D). Representative immunocytochemistry on cell culture inserts for junction protein Cldn5. (E–F) qPCR analysis of junction markers (E) and the Wnt target gene *Axin2* (F) in EC cultivated with AC from Evi^{Ctrl} or Evi$^{\Delta AC}$. EC culture alone is used as reference, * significant compared to EC alone, n = 5 except for Cldn5 for which n = 4.

co-culture of MBMECs with Evi$^{\Delta AC}$ ACs did not reduce TEER values in a paired analysis with co-cultures of MBMECs and Evi^{Ctrl} ACs, but rather tend to be slightly increased (Fig. 5B). The Ccl values instead were comparable (Fig. 5C). In line with these observations, we did not find differences in junctional staining for Cldn5 between Evi^{Ctrl} and Evi$^{\Delta AC}$ AC co-culture, whereas compared to MBMECs alone the co-culture with ACs resulted in a more pronounced junctional localization of Cldn5, as indicated by lower Ccl values (Fig. 5C, D). Opposed to this, the mRNA expression of Ocln but not Cldn5 was significantly decreased in the co-cultures compared to the mono-culture, whereas Cdh5 expression was comparable to MBMECs alone (Fig. 5E). Similarly, the expression of the Wnt target gene Axin2 did not significantly differ between the conditions, although in trend the co-culture with Evi^{Ctrl} ACs showed the highest value, indicative of higher Wnt stimulation, which in the co-culture with Evi$^{\Delta AC}$ ACs was almost at the level of the EC mono-culture (Fig. 5F).

In order to clarify if the increased brain water content and tracer permeability observed in Evi$^{\Delta AC}$ mice *in vivo* may result from augmented transcellular transport rather than from junctional opening, we analysed cortical microvessels by electron microscopy for vesicle formation and transcytotic activity. In 10-week-old mice, no significant difference of vesicle formation could be identified (data not shown). However, in 40-week-old mice we observed an increase of vesicles in cortical microvascular ECs from Evi$^{\Delta AC}$ mice (Fig. 6A). To quantitatively characterize

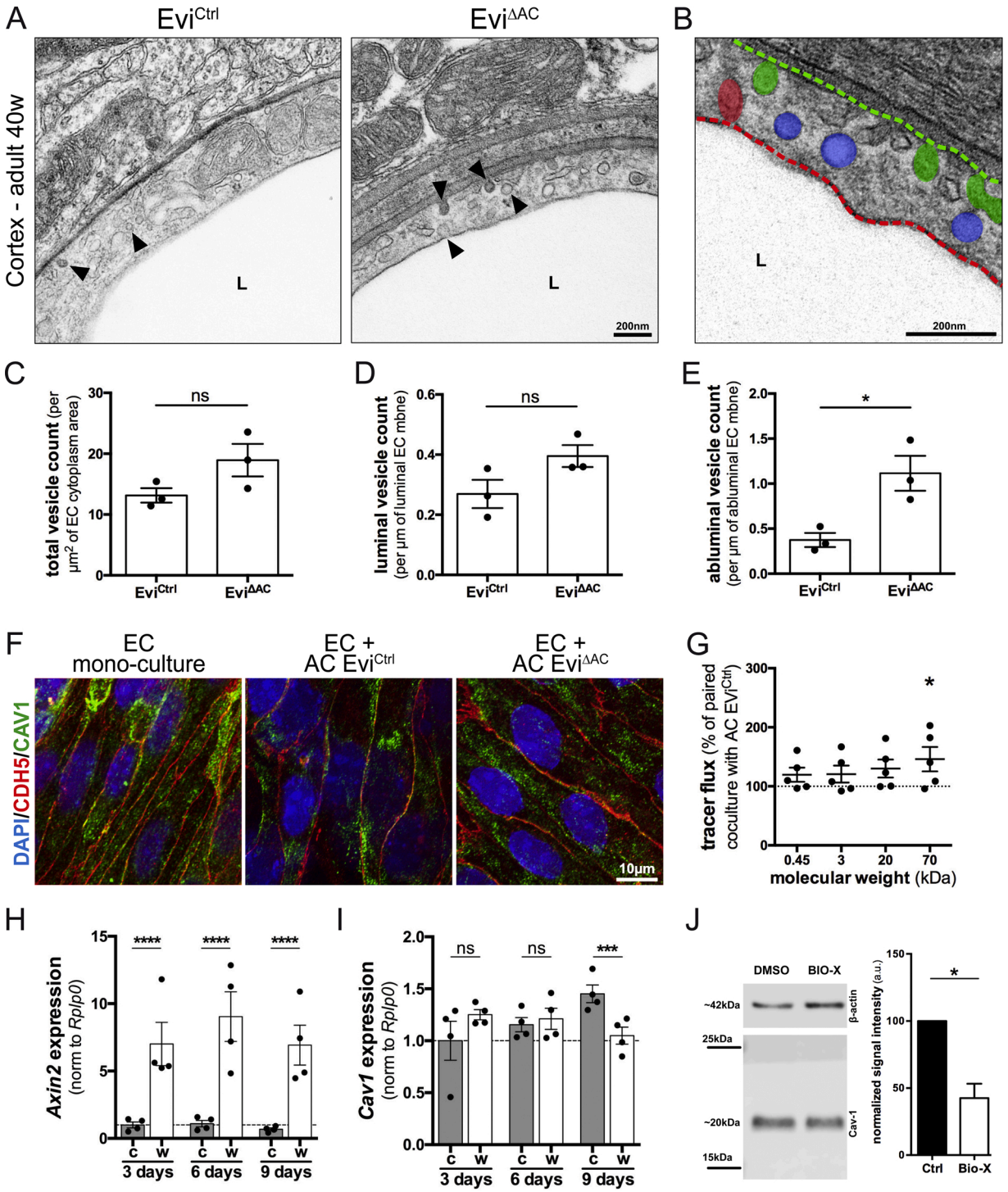

Fig. 6. Increased endothelial vesicles at the BBB of Evi$^{\Delta AC}$ mice.
(A) Electron microscopy images depicting the endothelial vesicles in cortical ECs of 40-week-old Evi^{Ctrl} and Evi$^{\Delta AC}$ animals and (B) High resolution image of endothelial vesicles in Evi$^{\Delta AC}$ mice and schematic representation of measurements for quantification. Red dashed line, luminal membrane length; red shape, luminal vesicles; blue shape, cytoplasmic vesicles; green shape, abluminal vesicles; green dashed line, abluminal membrane length. (C) Quantification of total vesicles performed on 12–19 4 µm diameter vessels analysed per animal and normalized to the endothelial cytoplasmic area, n = 3. (D) Quantification of luminal vesicle numbers performed on 12–19 images per animal and normalized to the endothelial membrane length, n = 3. (E) Quantification of abluminal vesicle numbers performed on 12–19 images per animal and normalized to the endothelial membrane length, n = 3. (F) Representative immunocytochemistry on cell culture inserts for Caveolin 1 (green). Cdh5 (red) is used to reveal cell-cell junctions. (G) *In vitro* permeability assay using the experimental setup presented in Fig. 5A and analysed after 3 h of incubation, n = 5. (H–I) qPCR analysis of the Wnt target genes *Axin2* (H) and the vesicle marker *Caveolin-1* (I) in EC monolayers treated with Wnt3a (w) or control medium (c) during 3; 6 or 9 days. (J) Western blot for Cav-1 upon Wnt/β-catenin activation by GSK3β inhibition with Bio-X (2.5µM, 24 h) in PBMECs (n = 3).

vesicle distribution, we analysed total, luminal and abluminal vesicles (Fig. 6B). Although there was a trend of an increased total as well as of luminal vesicles number in the Evi$^{\Delta AC}$ mice, the differences were not significant (Fig. 6C, D). However, abluminal vesicles were significantly increased in number, suggesting an intensified vesicle activity in brain ECs of Evi$^{\Delta AC}$ mice (Fig. 6E). As suggested by the MACE-Seq analysis, caveolae-mediated vesicular transport-related genes were increased in Evi$^{\Delta AC}$ mice compared to controls (Fig. 4F). In line with this, in the co-culture paradigm, an increase in Cav-1 staining, similar to the mono-culture condition, was observed in EC co-culture with ACs from Evi$^{\Delta AC}$ mice (Fig. 6F). Interestingly, permeability assays with differently sized tracers, ranging from 0.45–70 kDa performed at the experimental endpoint on the same inserts of the TEER measurement, revealed no difference between the Evi^{Ctrl} and Evi$^{\Delta AC}$ AC co-cultures after 1 h incubation (data not shown). However, after 3 h of incubation, co-cultures with Evi$^{\Delta AC}$ ACs showed a significantly increased permeability for 70 kDa dextran, whereas smaller tracers revealed only a similar trend (Fig. 6G). These data suggest that also *in vitro* an increase in endothelial transcellular permeability in Evi$^{\Delta AC}$ mice could be recapitulated by the MBMEC and AC co-culture model of the BBB.

In order to investigate if Cav-1 is directly regulated downstream of the Wnt/β-catenin pathway, we performed a time series of recombinant Wnt3a (150 ng/mL) applications on MBMECs and analysed by qRT-PCR the regulation of Axin2 and Cav-1 at 3, 6 and 9 days of stimulation. Robust Axin2 upregulation at all three time points confirmed activation of β-catenin transcriptional activity upon Wnt3a treatment (Fig. 6H). Along with the duration of the culture of MBMECs, Cav-1 expression increased from 3 to 9 days in the control condition, whereas Cav-1 levels were significantly lower in the Wnt3a-treated cells at 9 days of culture (Fig. 6I). Due to the limited availability of MBMECs, we performed a comparable experiment in primary porcine brain microvascular endothelial cells (PBMECs) that can be grown in large quantities. PBMECs were treated with 2.5μM of the GSK3 inhibitor BIO-X for 24 h, leading to β-catenin stabilization. Total protein was isolated from PBMECs and subjected to western blot analysis, revealing significantly down-regulated Cav-1 upon GSK3 inhibition, hence β-catenin transcriptional activity (Fig. 6J).

3.5. Astrocytic end-feet but not pericytes are affected in Evi$^{\Delta AC}$ mice showing altered morphology and Aqp4 distribution

As release of Wnt growth factors from ACs is abolished in our model, we systematically analysed the composition and morphology of the cellular compartments of the NVU. Pericytes were shown to have major functions in controlling BBB integrity and their ablation from the NVU results in increased vesicular transport across brain microvascular ECs, as well as in abnormal polarization of astrocytic end-feet and ACs detachment (Armulik et al., 2010; Daneman et al., 2010).

Consequently, we first analysed the coverage of brain microvessels by CD13-positive PCs in young (10 weeks) and middle-aged (40 weeks) adult Evi$^{\Delta AC}$ and Evi^{Ctrl} mice (Fig. S8A). Interestingly, PC coverage of cortical brain microvessels, evidenced as percent PC volume of CD31^{+} vessel volume, was not significantly affected at either age in Evi$^{\Delta AC}$ mice. A comparable observation was made for the other brain regions analysed (Fig. S8B, C, F, G). Instead, when the pericyte number was analysed by counting the PC cell bodies normalized to the vessel volume, it became apparent, that specifically in 10-week-old Evi$^{\Delta AC}$ mice the number was lower than in Evi^{Ctrl} (Fig. S8D, E). In 40-week-old mice, in most brain areas the PC cell numbers were on the same level in Evi$^{\Delta AC}$ and Evi^{Ctrl} mice (Fig. S8H, I). It is of note that at 10 w, Evi^{Ctrl} mice showed a significantly higher level of PC cells attached to blood vessels than at 40 w, which might suggest that the PC numbers regress during ageing in the controls, whereas in the Evi$^{\Delta AC}$ mice the relative PC cell number per vessel remains virtually unchanged between 10- and 40-week-old mice.

We further analysed the coverage of brain microvessels by astrocytic end-feet *via* staining of the astrocytic water channel aquaporin-4 (Aqp4), which is a structural component of the end-foot membrane (Nagelhus et al., 2004) (Fig. 7). Analysis of the Aqp4 staining volume, normalized to the vessel volume evidenced by CD31 staining, revealed that in 40 w mice Aqp4 was significantly increased in cortical and SVZ vessels (Fig. 7A, C). To a lesser extent this effect was already observed as a trend in 10 w animals in cortical vessels only (Fig. 7B).

Moreover, detailed analysis of the cortical vessels showed that Aqp4 staining resulted in more background and diffuse labelling appearance in the Evi$^{\Delta AC}$ mice (Fig. 7A). Specifically, the structure of the staining was not smooth along the vessel wall as in the Evi^{Ctrl} mice but showed dotted areas around the vessel outline that are highlighted by the volume rendering of high magnification images (Fig. 7D, arrowheads).

To better understand the morphological consequences of the changes observed in Aqp4, we subjected cortical brain tissue of Evi$^{\Delta AC}$ and Evi^{Ctrl} mice to electron microscopic analysis. In young adult animals (10 weeks), alterations of astrocyte endfeet were already detectable, but less frequently observed in Evi$^{\Delta AC}$ mice compared to controls (data not shown). In middle-aged (40 weeks) mice, swollen astrocytic end-feet were frequently detected by electron microscopy, supporting the initial observation of increased brain water content due to cytotoxic oedema as well as Aqp4 mislocalization (Fig. 7E).

Interestingly, ACs isolated from Evi$^{\Delta AC}$ mice showed significantly lower expression levels of the Wnt/β-catenin target genes Axin2 and Nkd1, suggesting that the deletion of Wnt factor release from astrocytes affects autocrine stimulation (Fig. 7F and G). It is of note that the expression of the non-Wnt-related ligand Ndp remained stable in ACs, suggesting that Evi deletion does not lead to a compensatory upregulation of Ndp (Fig. 7H).

3.6. Evi$^{\Delta AC}$ mice show elevated neuronal activity in the lateral septal nucleus, indicative for physiological downstream effects of augmented BBB permeability in vivo

In order to understand if the moderate brain oedema and the increase in transcellular permeability as well as astrocyte end-feet swelling in Evi$^{\Delta AC}$ mice may result in altered neuronal function, we analysed the brains of Evi$^{\Delta AC}$ and Evi^{Ctrl} mice for c-fos reactivity by immunohistochemistry (Fig. 8). By screening of the brains at the two different sectioning levels related to bregma, we observed a trend of increased nuclear c-fos staining in neurons of the lateral septal nucleus (LSN) of Evi$^{\Delta AC}$ mice at 10 weeks-of-age, which was significantly increased in 40-week-old mice (Fig. 8A top, B, D). Although the relative c-fos reactivity appeared to be decreased with age, the difference between Evi$^{\Delta AC}$ and control mice was particularly strong in the 40-week-old group, suggesting that the age-related increased in permeability correlated with an alteration of neuronal activity in the LSN. Additionally, and only in 40-week old animals, neuronal activation was also increased in the periventricular thalamus (PVT) and the intermedio-dorsal thalamic nucleus (IMD) (Fig. 8A bottom, C, E). Although Evi$^{\Delta AC}$ mice are viable and have no gross morphological and behavioural deficits, the slight brain oedema and overall increased transcellular permeability of ECs might lead to a modulation neural activity, potentially resulting in discrete/subtle behaviour modifications later in life of these animals.

4. Discussion

Astrocytes (ACs), an essential cellular component of the neurovascular unit (NVU). They have been shown to support the formation and integrity of endothelial barrier function known as the blood-brain barrier (BBB). The intimate connection between cells at the NVU is important for their communication *via* signalling pathways relevant for BBB formation and maintenance. The Wnt/β-catenin pathway, mediated in particular by the ligands Wnt7a/7b, is accepted to be crucial for brain angiogenesis, as well as for barriergenesis and BBB maintenance (Blanchette and Daneman, 2015; Daneman et al., 2009; Liebner et al.,

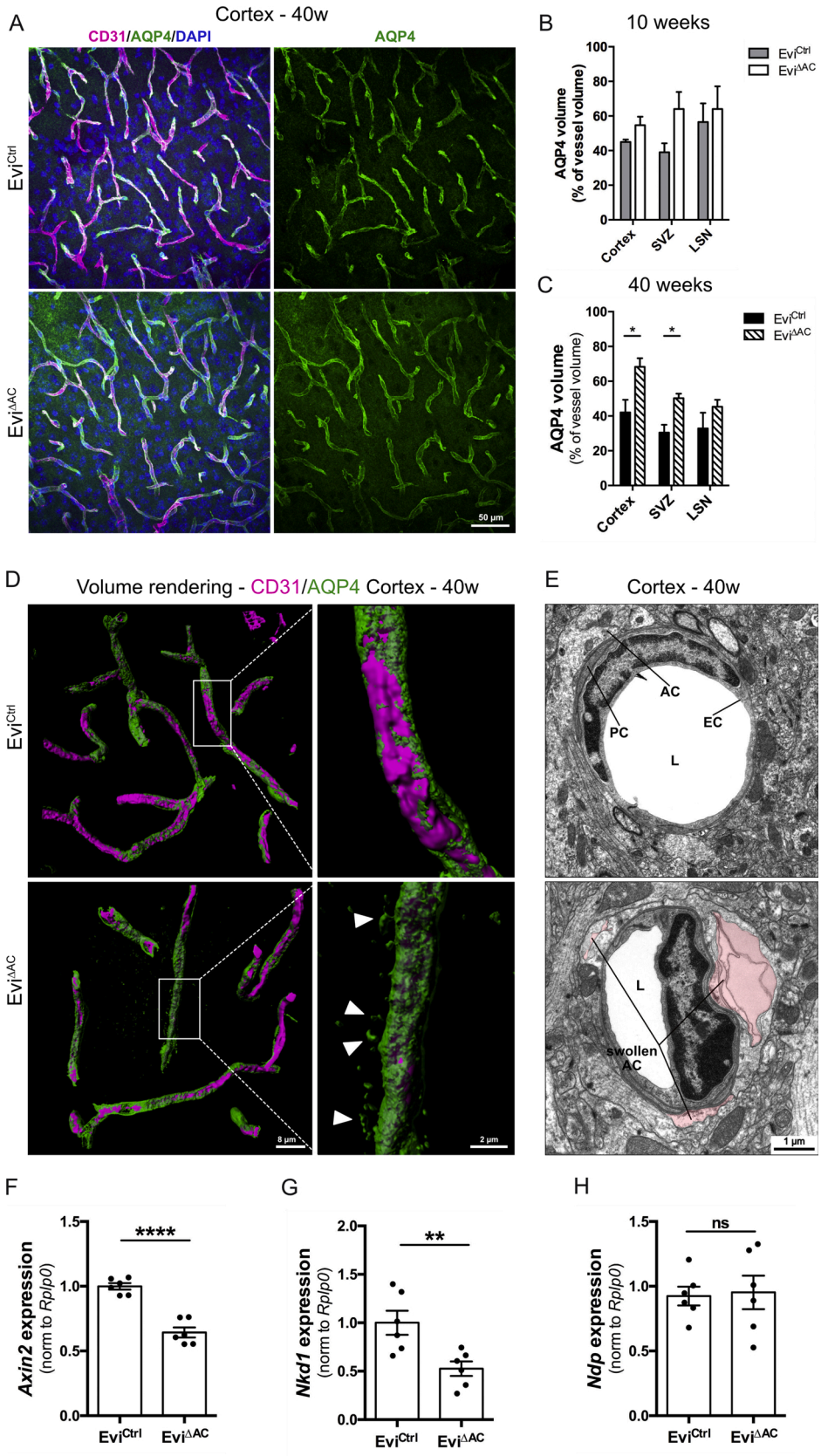

Fig. 7. Astrocyte endfeet volume is increased in Evi$^{\Delta AC}$ animals.
(A) Representative pictures of cortical vessels (CD31, magenta) in 50 µm sections covered by astrocyte end-feet (AQP4, green) in of 40-week-old Evi^{Ctrl} and Evi$^{\Delta AC}$ animals (B–C) Quantification of AQP4 volume in different regions at bregma 0.98 mm for (B) 10-week and (C) 40-week-old Evi^{Ctrl} and Evi$^{\Delta AC}$ animals, n = 3. (D) Volume rendering of confocal microscopy of the AQP4 staining around vessels. White arrowheads point to mis-localised Aqp4 in Evi$^{\Delta AC}$ animals. (E) Transmission electron microscopy of astrocyte endfeet in cortex of 40-week-old Evi$^{\Delta AC}$ animals. Representative image of n = 3. (F–H) qPCR analysis of the Wnt target genes (F) *Axin2*, (G) *Nkd1* and (H) *Ndp* in ACs isolated from Evi^{Ctrl} and Evi$^{\Delta AC}$ animals. Primary AC culture passage 1, n = 6.

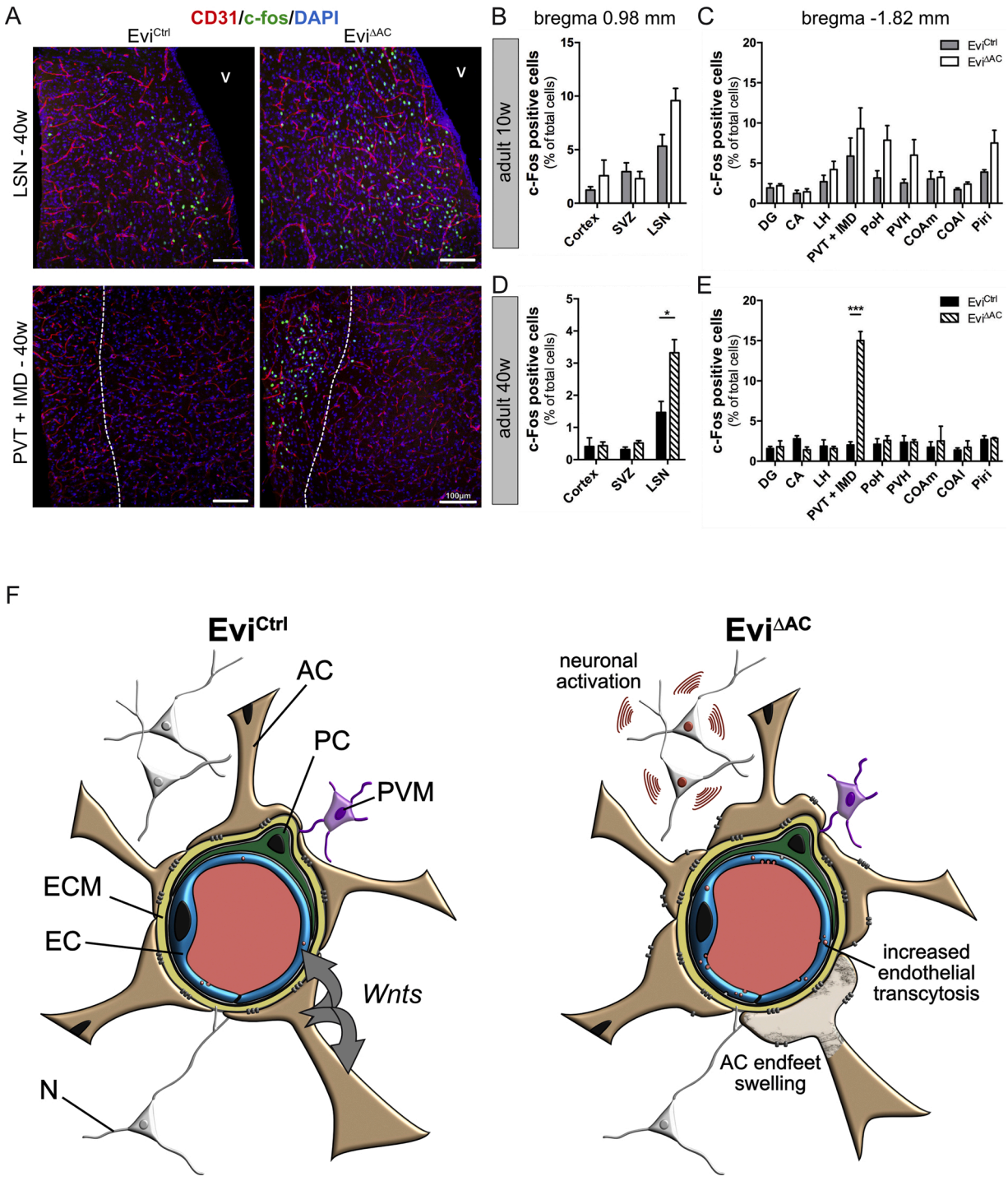

Fig. 8. Neuronal activation is increased in Evi$^{\Delta AC}$ animals.
(A) Representative images of activated neurons (c-fos, green) and vessels (CD31, red) stained in 10 µm sections for LSN and PVT + IMD regions of 40 w old Evi^{Ctrl} and Evi$^{\Delta AC}$ mice. (B–E) Quantification of c-fos positive cells in different regions of the brain for (B–C) 10-week and (D–E) 40-week-old animals, n = 3. (F) Schematic view of the modifications observed in Evi$^{\Delta AC}$ compared to Evi^{Ctrl} animals.

2008; Stenman et al., 2008; Vanhollebeke et al., 2015; Zhou et al., 2014b). Given that the potential cellular sources for Wnt growth factors in the established NVU of adult mammalian organisms are limited and that conclusive data are missing (Cheslow and Alvarez, 2016), we have addressed the question if AC-derived Wnt growth factors contribute to BBB maintenance in adult mice.

In the present manuscript we show that Wnt growth factors released by ACs are required for BBB maintenance and structural integrity of AC end-feet at the NVU. We inactivated Wnt secretion specifically in ACs *via* hGFAP-Cre-mediated deletion of the *eveness interrupted* (Evi) gene, that is mandatory for the release of all Wnt growth factors (Bänziger et al., 2006). Deletion of the Evi gene in the majority of ACs (Fig. 1B and S2) in Evi$^{\Delta AC}$ mice did not lead to prominent vascular alterations, cerebral bleeding or a lethal phenotype, suggesting that the function of AC-derived Wnts could largely be compensated. However, at adult stages, the AC-specific Evi knock out led to a) an increased brain water content and tracer extravasation, as well as reduced PCs counts at vessels in young adult mice (10 weeks), b) a reduction in Wnt pathway

target gene expression in ECs and ACs (10 and 40 weeks), c) an increased endothelial vesicular abundance in middle-aged adult mice (40 weeks), d) AC end-feet swelling with mis-localised Aqp4 (40 weeks), and e) increased neuronal activation in the LSN, the PVT and the IMD (40 weeks). These findings were not gender-specific when we separated permeability results for male and female (data not shown). Although for a clear-cut statement a detailed and dedicated gender analysis would be required. Taken together, these data consistently suggest that in the adult the release of Wnt growth factors from ACs is required to maintain the integrity of the NVU and of astrocytic end-feet in particular.

4.1. Specificity of hGFAP-Cre-mediated recombination for mouse brain astrocytes

Although GFAP is first detectable around 9.5dpc, its robust expression is detected in the mouse brain from 15.5dpc to birth coinciding with the differentiation of astrocytes (Fox et al., 2004; Morita et al., 1997). Therefore, the earlier expression of GFAP is related to other cell types, in particular to radial glia and neural precursor cells (Briona et al., 2015; Casper and McCarthy, 2006). Moreover, it has been shown for a comparable hGFAP-GFP line that the human GFAP promoter presents regional heterogeneity regarding its activity in the mouse brain (Moon et al., 2011). Consequently, hGFAP-mediated deletion of Evi likely takes place also in other cell types and may not be induced in all ACs homogeneously. However, at least in the zebrafish it has been shown for the hypothalamic region that Wnt signalling in radial glia and neural stem and precursor cells is not required for their proliferation and differentiation (Duncan et al., 2016). As we have not observed any gross morphological alterations in the $Evi^{\Delta AC}$ mice, we came to the conclusion that the hGFAP-Cre:$Evi^{fl/fl}$ mouse model mainly affects the differentiation and function of astrocytes. Still, it is possible that the $Evi^{\Delta AC}$ mice might exhibit some defects in other cell types and brain regions that we did not investigate. Additionally, the observation that the BBB phenotype aggravated with age might be related to increased GFAP expression in ACs during ageing, which has been shown for the hippocampus of control and senescence-accelerated-prone mice (Wu et al., 2005). Therefore, adult neurogenesis in the subventricular zone (SVZ) (Garcia et al., 2004), ageing-related defects (Wu et al., 2005) or conditions of regeneration after injury (Briona et al., 2015), for which GFAP expression and Wnt/β-catenin signalling have been described might be interesting to analyse in the future.

4.2. Astrocytic contribution to barrier signals in adult mice

During embryonic vascularization of the neuroectoderm, when endothelial Wnt signalling is prominent, the growth factors Wnt7a and Wnt7b are known to be released by neural precursor cells (NPCs), inducing specific endothelial β-catenin transcriptional activation (Blanchette and Daneman, 2015; Eubelen et al., 2018; Reis and Liebner, 2013; Zhou and Nathans, 2014). In parallel, Ndp, a factor unrelated to Wnts, is also able to activate β-catenin transcription which however, appears to be specific for the cerebellum and the retina as part of the CNS (Junge et al., 2009; Ye et al., 2009). Although it has been shown that the Wnt pathway is instrumental in maintaining endothelial BBB function in the adult mammalian and teleost brain, the source of Wnt growth factors remains elusive (Zhou and Nathans, 2014). With the rapid decline in NPCs during postnatal stages, barrier-maintaining signals are likely to be released from other cell types. While pericytes (PCs) are crucial for BBB integrity (Armulik et al., 2010; Daneman et al., 2010), a recent single cell sequencing study on the molecular identity of brain vascular cells suggests that PCs and smooth muscle cells (SMCs) neither express Wnt7a/7b, nor Ndp (Vanlandewijck et al., 2018). Instead, the main source of Wnts and Ndp are ACs with minor contribution from the newly described vascular fibroblast-like cells. Astrocytes start to differentiate from neural precursor cells at late gestation stages in the mouse, in a process that persists for several weeks, up to one month after birth (Bayraktar et al., 2015; Qian et al., 2000). We could confirm broad expression of Wnt growth factors by ACs compared to whole brain or MBMECs mRNA by quantitative RT-PCR (Fig. S1). What became also apparent in the RT-PCR analyses is that ACs express the entire receptor and co-receptor machinery allowing them to respond to Wnt signals potentially in an autocrine manner. Moreover, ACs also express sonic hedgehog (Shh) as well as angiopoietin-1 (Ang-1) that have been shown to contribute to BBB integrity and stability under chronic inflammatory conditions (data not shown) (Alvarez et al., 2011; Gurnik et al., 2016).

Recombination of ACs by hGFAP-driven Cre activity (Fig. S2) results in an almost complete knock out of Evi, as evidenced by ~90% down-regulation of its mRNA in cultured cortical ACs (Fig. 1B). As suggested by the analysis of isolated cortical capillary fragments, Wnt/β-catenin pathway activation is indeed suppressed in the neurovascular unit indicated by the significant downregulation of the Wnt target genes Axin2 and Nkd1 in 40-week-old mice (Fig. 2B). While Glut-1, as another canonical Wnt target, appears to be upregulated on the mRNA level in FACS-sorted ECs by MACE-Seq analysis, we could not detect differences in protein expression and/or distribution (Figure S4C).

Here we show that interfering with Wnt growth factor release from ACs, by conditional deletion of Evi in GFAP-expressing cells, is not compensated by significant changes in the expression of other BBB-promoting growth factors such as Ndp (Fig. 7H).

4.3. Wnt release from ACs has only little impact on EC junctions

Given the increase in brain water content and in brain permeability upon Evi deletion in ACs, we initially interpreted this as an opening of BBB junctions, ultimately leading to a mild brain oedema and tracer leakage, respectively (Fig. 1C-J). Indeed, mRNA expression of VE-cadherin (Cdh5) as well as ZO-1 were down-regulated in MBMVs from middle-aged (40 weeks) $Evi^{\Delta AC}$ mice, supporting the interpretation that junctions are affected to some extent by Evi deletion in ACs (Fig. 2C). Instead, RNA-Seq from FACS-isolated ECs, revealed an “activated” angiogenic-like expression profile with no obvious downregulation of tight junction genes (Fig. 4E). Specifically, Cdh5 turned out to be upregulated in $CD31^+$ FACS-sorted ECs, which, at first glance, might be contradictory to the MBMV results. However, it could be in line with previous reports, showing increased Cdh5 expression in immature brain ECs that becomes reduced during BBB maturation (Breier et al., 1996). Moreover, the differences in the isolation procedure for MBMVs and $CD31^+$ ECs by FACS-sorting may explain the discrepancies of individual gene regulation.

Further analysis of regulated genes by western blotting confirmed a significant downregulation of Cdh5 in the vessel fragments (Fig. S4A). However, qualitative and quantitative analyses of Cdh5, Cldn5 (Fig. 3 and S5), as well as ZO-1 (data not shown) localization in brain did not reveal apparent differences between $Evi^{\Delta AC}$ and Evi^{Ctrl} mice. *In vitro* experiments also supported the interpretation that the abrogation of the Wnt release from ACs has only minor effects on inter-endothelial junctions. Indeed, co-cultures of MBMECs with ACs derived from $Evi^{\Delta AC}$ and Evi^{Ctrl} mice did not lead to different expression and/or localization of junctional proteins such as Cdh5 or Cldn5 (Fig. 5D, E and 6 F). Moreover, TEER measurement, which is a marker for junctional tightness, revealed a trend of increased resistance values in MBMECs co-cultured with ACs from $Evi^{\Delta AC}$ mice compared to controls (Fig. 5B). This suggests that over all the junctional effects are minor and may not explain the increased permeability in $Evi^{\Delta AC}$ mice. Along with this observation it is of note that although the Wnt target Axin2 was in trend decreased, it was not significantly diminished in MBMECs co-cultured with $Evi^{\Delta AC}$. In this regard, the prime suspect for functional compensation of paracellular barrier maintenance could still be Ndp, which is released by ACs even in the absence of Evi and is able to activate endothelial β-catenin (Junge et al., 2009; Ye et al., 2009). Our data however support the hypothesis that Ndp might not rescue the entire spectrum of functions of

Wnt signalling in Evi$^{\Delta AC}$ mice, given the fact that knock out animals develop brain oedema and increased transcellular transport (Fig. 1).

In this regard it is important to note that previous publications by us and others demonstrated the role of β-catenin-mediated Wnt signalling specifically in CNS ECs, by endothelial gain- or loss-of-function models. The same is true for publications revealing the receptor involvement for Wnt pathway activation in ECs (Benz et al., 2019; Daneman et al., 2009; Liebner et al., 2008; Posokhova et al., 2015; Stenman et al., 2008; Vanhollebeke et al., 2015; Zhou and Nathans, 2014; Zhou et al., 2014a). In the present study we abolished the secretion of Wnts by the deletion of the Evi gene in the ACs only. Therefore, the milder phenotype observed in Evi$^{\Delta AC}$ mice compared to previous approaches, might be explained on the one hand by an incomplete knock out of about 10% (Fig. 1B) and on the other hand by the possibility that other cells of the NVU may take over Wnt or Ndp secretion.

Moreover, in Evi$^{\Delta AC}$ animals, not only secretion of canonical Wnts is affected, but also of non-canonical ligands which are known to activate the planar cell polarity (PCP) and Ca^{2+} signalling pathways. Interestingly, canonical and non-canonical Wnts can exert opposing effect in various cells and organism, which may contribute to the overall phenotype we observed in Evi$^{\Delta AC}$ mice (Lezzerini and Budovskaya, 2014; Sato et al., 2010).

4.4. ECs show an activated expression profile and increased transcellular transport

As the oedema and permeability phenotypes could not be explained by junction disruption, we isolated MBMECs from cortex of adult Evi^{Ctrl} and Evi$^{\Delta AC}$ by flow cytometry to have a broader insight in transcription profile alterations. By the MACE transcriptional profiling it became apparent that brain ECs from Evi$^{\Delta AC}$ exhibit an angiogenic-like profile compared to those of Evi^{Ctrl} (Fig. 4 and S7). Although endothelial differentiation genes as well as several ECM genes like Lama5 turned out to be upregulated in the Evi$^{\Delta AC}$ mice, staining for Lama5 did not corroborate this on the level of protein distribution in cortical sections of 10- and 40-week-old mice (Fig. S6). Moreover, the angiogenic-like gene profile did not coincide with increased vascular density and branching in various brain regions (Fig. S3). However, the transcriptomic analysis further revealed a group of regulated genes related to caveolae (Fig. 4F). Interestingly, we observed an increase in vesicle numbers in cortical brain ECs of middle-aged (40 week) Evi$^{\Delta AC}$ animals (Fig. 6A-E). In line with the *in vivo* observation, MBMECs presented reduced Cav1 staining upon coculture with Evi^{Ctrl} ACs, which was not visible in case of Evi$^{\Delta AC}$ ACs (Fig. 6F). The latter finding coincided with an increased permeability to high molecular weight tracers (Fig. 6G). Additionally, we provide evidence for an inhibitory function of the Wnt/β-catenin pathway on the expression of Cav-1. MBMECs were stimulated *in vitro* for 9 days with recombinant Wnt3a or PBMECs were stimulated with BIO-X for 24 h, demonstrating reduced expression of Cav-1 upon Wnt pathway activation (Fig. 6H-J). Similarly, it has been shown in experimental autoimmune encephalomyelitis (EAE), a mouse model for multiple sclerosis, that inactivation of Wnt/β-catenin signalling exacerbates the clinical presentation of mice by increasing Cav-1-mediated transcellular transport (Lengfeld et al., 2017). In line with this, Cav-1 can inhibit Wnt/β-catenin signalling by sequestering β-catenin at caveolae membrane domains in 3T3 cells (Galbiati et al., 2000). Instead, dominant activation of Wnt/β-catenin signalling in ECs diminishes vesicular transport and Cav-1 expression in leaky vessels of the circumventricular organs (Benz et al., 2019; Y. Wang et al., 2019). On the other hand, a certain amount of Cav-1 might also be required for proper Wnt signalling and consequently for BBB maintenance, as activation of the Wnt/β-catenin pathway *via* internalization of Lrp6 requires expression of Cav-1 in non-endothelial cells (Yamamoto et al., 2006). In the light of these published data, our work supports the interpretation that in adult mice, Wnt factors secreted by ACs are crucial for maintaining low transcellular vesicular traffic by limiting Cav-1 expression in brain ECs to a physiological state. In the absence of Wnt ligand availability, as in the Evi$^{\Delta AC}$ condition, upregulated Cav-1 cannot support Fzd/Lrp-mediated signalling but might exclusively mediate vesiculation, thereby increasing BBB transcellular permeability.

The increase in trans-endothelial transport likely also mediates the increased tracer permeability and mild oedema formation in the Evi-deficient mice. In this regard it has been reported that the *Major Facilitator Superfamily Domain Containing 2A* (Mfsd2a) regulated vesicular transport in ECs of the CNS by establishing a unique lipid composition of the plasma membrane that inhibits vesicle formation (Andreone et al., 2017; Ben-Zvi et al., 2014). Interestingly, the canonical Wnt pathway was recently shown to influence the lipid metabolism together with Myc in the context of hepatocellular carcinoma, in which Wnt/Myc increased the fraction of poly-unsaturated fatty acyl groups in a Ras-dependent manner (Yao et al., 2018). Although we could not identify an altered regulation of Mfsd2a expression in Evi$^{\Delta AC}$ mice (data not shown), it will be interesting to address the interaction of Wnt and lipid metabolism in brain ECs in future investigations.

4.5. PC coverage and astrocyte end-feet integrity is impaired in Evi$^{\Delta AC}$ mice, leading to altered neuronal activity

It is worth noting that the NVU is composed of at least five or six cell types - if fibroblast-like cells are included - all of which might be influenced by the deletion of Evi in ACs. Isolated MBMVs that were used in the present work contained at least 3 cell types including ECs, PCs, and AC end-feet. Consequently, the downregulation of Wnt targets observed in qRT-PCR analysis (Fig. 2B) might be derived from other cells than ECs. This interpretation is supported by the finding that isolated ACs from Evi$^{\Delta AC}$ mice also showed a down-regulation of the tested Wnt targets (Fig. 7F, G). Furthermore, astrocytic end-feet integrity became severely impaired upon the persistent lack of Wnt factor release from ACs in 40-week-old mice. Specifically, Aqp4 showed a broader area around the vessels, which is in line with its delocalization, as well as with end-feet swelling, and signs of disintegration evidenced by electron microscopy (Fig. 7A-E). Regarding the AC end-feet phenotype, it has been shown that AQP4 promotes cytotoxic oedema formation in case of water intoxication (Manley et al., 2000). Therefore, these data could explain the oedema and astrocyte end-feet swelling we observed in our experimental model. However, AQP4 also has protective effects in case of vasogenic oedema and may reduce oedema-associated epileptic events (Bloch and Manley, 2007). How the AC-specific deletion of Evi might influence the outcome of the diseased brain like in stroke, will be subject to future investigations.

In young adults (10 weeks), reduced PC numbers at vessels appear to precede the AC end-feet phenotype (Fig. S8). Given that in middle-aged mice, no major differences in PCs could be observed, we concluded that PC coverage might be affected only during early postnatal maturation of brain vessels, potentially contributing to increased permeability that we observed in young adult (10 weeks) Evi$^{\Delta AC}$ mice. This interpretation fits to observations made in PC-deficient mice, in which the lack of PCs leads to increased tracer permeability in ECs, mediated by elevated transcytosis (Armulik et al., 2010). In turn, PC-deficient mice also develop an AC end-feet phenotype, similar to the one we described in Evi$^{\Delta AC}$ mice, hence opening the possibility that AC-PC interaction may in part be controlled by AC-derived Wnt factors.

Ultimately, our findings may support the interpretation that the end-feet phenotype in astrocytes results from the reciprocal interactions between the cells of the NVU specifically, between ECs, PCs and ACs. Moreover, ACs may require autocrine Wnt signals to maintain end-feet integrity and consequently support BBB function in ECs at the NVU. This interpretation is supported by the observation that ACs express almost the entire set of frizzled receptors and Lrp co-receptors (Fig. S1) and that the Wnt target gene Axin2 and Nkd1 were downregulated in ACs from Evi$^{\Delta AC}$ mice *in vitro* (Fig. 7F and G).

Finally, we observed increased c-fos reactivity in the lateral septal

nucleus (LSN) in 40-week-old Evi$^{\Delta AC}$ animals, although spontaneous mouse behaviour was not altered (Fig. 8). The LSN region takes part in the regulation of processes linked to social behaviour, especially to anxiety and stress (Kim and Han, 2016; Mesic et al., 2015; Talishinsky and Rosen, 2012). Moreover, in middle-aged mice (40 weeks), two nuclei of the thalamus (PVT and IMD) also exhibit enhanced c-fos reactivity in Evi$^{\Delta AC}$ mice. Defined by their projections to different brain areas, these regions were shown to affect fear-related memory and alcohol/drug addiction among others (Gupta et al., 2018; Mátyás et al., 2014; Paydar et al., 2014; Penzo et al., 2015). Therefore, it would be interesting to test in future studies if the stress and fear response is modified in Evi$^{\Delta AC}$ mice. Moreover, these findings might be also relevant for understanding the crosstalk between vessels and neurons in general, given the recently published work by Chow and colleagues, showing that Cav-1 in brain arterioles is required for neurovascular coupling (Chow et al., 2020).

5. Conclusion

In this study, we show by inhibiting the release of Wnt growth factors from astrocytes (ACs) *via* the cell-specific deletion of the Evi gene in mice (Evi$^{\Delta AC}$), that AC-derived Wnts are required to maintain the integrity of the neurovascular unit (NVU) and consequently of endothelial blood-brain barrier (BBB) function. Evi$^{\Delta AC}$ mice exhibit a progressive loss of endothelial barrier properties, evidenced by increased tracer permeability and oedema formation in adults. We observe that brain ECs of Evi$^{\Delta AC}$ mice show increased expression of Cav-1 and significantly augmented vesicular abundance, but no detectable changes in junctional integrity. We further demonstrate that during ageing of Evi$^{\Delta AC}$ mice, an initial decrease in pericyte number (10 w) at brain vessels is followed by astrocytic end-feet alterations with mislocalisation of the water channel Aqp4, concomitant with a loss of end-feet structural integrity. Therefore, ACs might require - like previously shown for ECs (Zhou et al., 2014b) - sustained, low level autocrine Wnt/β-catenin signalling to maintain structural and functional integrity of the NVU and ultimately to maintain the physiological condition of the BBB.

Acknowlegements

S.L. was supported by the Deutsche Forschungsgemeinschaft SFB/TR23 "Vascular Differentiation and Remodeling", the research group FOR2325 "The Neurovascular Interface" (LI 911/5-1), the individual project LI 911/7-1 and the Excellence Cluster Cardio-Pulmonary Institute (CPI). From the European Union HORIZON 2020 ITN "BtRAIN", the German Centre for Heart and Circulation Research (DZHK, Column B: Shared Expertise) and by the LOEWE CePTER Epilepsy Research Center of the state Hesse. Thanks to Karl Heinz Plate and the Edinger Foundation for providing a stipend to B.H.Y. Additionally, B.H.Y. has been supported by a PhD grant from the Avicenna Foundation. Goethe International Postdoc Program (Go-In) was granted to S.G. (291776). Lama4 and Lama5 antibodies have been kindly provided by Lydia Sorokin (Institute of Physiological Chemistry and Pathobiochemistry, University of Münster, Germany). The hGFAP-Cre mice were kindly provided by David H. Gutmann (Washington University in St. Louis, MO USA), and the Evifl/fl mice were kindly provided by Richard A. Lang (The Visual Systems Group, Division of Pediatric Ophthalmology, Cincinnati Children's Hospital Medical Center, Cincinnati, United States).

Appendix A. The Peer Review Overview and Supplementary data

The Peer Review Overview and Supplementary data associated with this article can be found in the online version: https://doi.org/10.1016/j.pneurobio.2020.101937.

References

Alvarez, J.I., Dodelet-Devillers, A., Kebir, H., Ifergan, I., Fabre, P.J., Terouz, S., Sabbagh, M., Wosik, K., Bourbonnière, L., Bernard, M., van Horssen, J., de Vries, H. E., Charron, F., Prat, A., 2011. The hedgehog pathway promotes blood-brain barrier integrity and CNS immune quiescence. Science 334, 1727–7731. https://doi.org/10.1126/science.1206936.

Andreone, B.J., Chow, B.W., Tata, A., Lacoste, B., Ben-Zvi, A., Bullock, K., Deik, A.A., Ginty, D.D., Clish, C.B., Gu, C., 2017. Blood-brain barrier permeability is regulated by lipid transport-dependent suppression of caveolae-mediated transcytosis. Neuron 94, 581–594. https://doi.org/10.1016/j.neuron.2017.03.043 e5.

Armulik, A., Genové, G., Mäe, M., Nisancioglu, M.H., Wallgard, E., Niaudet, C., He, L., Norlin, J., Lindblom, P., Strittmatter, K., Johansson, B.R., Betsholtz, C., 2010. Pericytes regulate the blood–brain barrier. Nature 468, 557–561. https://doi.org/10.1038/nature09522.

Bajenaru, M.L., Zhu, Y., Hedrick, N.M., Donahoe, J., Parada, L.F., Gutmann, D.H., 2002. Astrocyte-specific inactivation of the neurofibromatosis 1 gene (NF1) is insufficient for astrocytoma formation. Mol. Cell. Biol. 22, 5100–5113.

Bänziger, C., Soldini, D., Schütt, C., Zipperlen, P., Hausmann, G., Basler, K., 2006. Wntless, a conserved membrane protein dedicated to the secretion of Wnt proteins from signaling cells. Cell 125, 509–522. https://doi.org/10.1016/j.cell.2006.02.049.

Bayraktar, O.A., Fuentealba, L.C., Alvarez-Buylla, A., Rowitch, D.H., 2015. Astrocyte development and heterogeneity. Cold Spring Harb. Perspect. Biol. 7, a020362–16. https://doi.org/10.1101/cshperspect.a020362.

Benz, F., Wichitnaowarat, V., Lehmann, M., Germano, R.F., Mihova, D., Macas, J., Adams, R.H., Taketo, M.M., Plate, K.H., Guérit, S., Vanhollebeke, B., Liebner, S., 2019. Low wnt/β-catenin signaling determines leaky vessels in the subfornical organ and affects water homeostasis in mice. Elife 8, 204. https://doi.org/10.7554/eLife.43818.

Ben-Zvi, A., Lacoste, B., Kur, E., Andreone, B.J., Mayshar, Y., Yan, H., Gu, C., 2014. Mfsd2a is critical for the formation and function of the blood–brain barrier. Nature 1–18. https://doi.org/10.1038/nature13324.

Blanchette, M., Daneman, R., 2015. Formation and maintenance of the BBB. Mech. Dev. 138, 8–16. https://doi.org/10.1016/j.mod.2015.07.007. Pt 1.

Bloch, O., Manley, G.T., 2007. The role of aquaporin-4 in cerebral water transport and edema. Neurosurg. Focus 22, E3.

Breier, G., Breviario, F., Caveda, L., Berthier, R., Schnurch, H., Gotsch, U., Vestweber, D., Risau, W., Dejana, E., 1996. Molecular cloning and expression of murine vascular endothelial-cadherin in early stage development of cardiovascular system. Blood 87, 630–641.

Briona, L.K., Poulain, F.E., Mosimann, C., Dorsky, R.I., 2015. Wnt/ß-catenin signaling is required for radial glial neurogenesis following spinal cord injury. Dev. Biol. (Basel) 403, 15–21. https://doi.org/10.1016/j.ydbio.2015.03.025.

Carpenter, A.C., Rao, S., Wells, J.M., Campbell, K., Lang, R.A., 2010. Generation of mice with a conditional null allele for Wntless. Genesis 48, 554–558. https://doi.org/10.1002/dvg.20651.

Casper, K.B., McCarthy, K.D., 2006. GFAP-positive progenitor cells produce neurons and oligodendrocytes throughout the CNS. Mol. Cell. Neurosci. 31, 676–684. https://doi.org/10.1016/j.mcn.2005.12.006.

Chang, J., Mancuso, M.R., Maier, C., Liang, X., Yuki, K., Yang, L., Kwong, J.W., Wang, J., Rao, V., Vallon, M., Kosinski, C., Zhang, J.J.H., Mah, A.T., Xu, L., Li, L., Gholamin, S., Reyes, T.F., Li, R., Kuhnert, F., Han, X., Yuan, J., Chiou, S.-H., Brettman, A.D., Daly, L., Corney, D.C., Cheshier, S.H., Shortliffe, L.D., Wu, X., Snyder, M., Chan, P., Giffard, R.G., Chang, H.Y., Andreasson, K., Kuo, C.J., 2017. Gpr124 is essential for blood-brain barrier integrity in central nervous system disease. Nat. Med. 23, 450–460. https://doi.org/10.1038/nm.4309.

Cheslow, L., Alvarez, J.I., 2016. Glial-endothelial crosstalk regulates blood–brain barrier function. Curr. Opin. Pharmacol. 26, 39–46. https://doi.org/10.1016/j.coph.2015.09.010.

Chow, B.W., Nuñez, V., Kaplan, L., Granger, A.J., Bistrong, K., Zucker, H.L., Kumar, P., Sabatini, B.L., Gu, C., 2020. Caveolae in CNS arterioles mediate neurovascular coupling. Nature 579, 106–110. https://doi.org/10.1038/s41586-020-2026-1.

Czupalla, C.J., Liebner, S., Devraj, K., 2014. In vitro models of the blood-brain barrier. Methods Mol. Biol. 1135, 415–437. https://doi.org/10.1007/978-1-4939-0320-7_34.

Daneman, R., Agalliu, D., Zhou, L., Kuhnert, F., Kuo, C.J., Barres, B.A., 2009. Wnt/beta-catenin signaling is required for CNS, but not non-CNS, angiogenesis. Proc. Natl. Acad. Sci. 106, 641–646. https://doi.org/10.1073/pnas.0805165106.

Daneman, R., Zhou, L., Kebede, A.A., Barres, B.A., 2010. Pericytes are required for blood-brain barrier integrity during embryogenesis. Nature 468, 562–566. https://doi.org/10.1038/nature09513.

Devraj, K., Klinger, M.E., Myers, R.L., Mokashi, A., Hawkins, R.A., Simpson, I.A., 2011. GLUT-1 glucose transporters in the blood-brain barrier: differential phosphorylation. J. Neurosci. Res. 89, 1913–1925. https://doi.org/10.1002/jnr.22738.

Devraj, K., Poznanovic, S., Spahn, C., Schwall, G., Harter, P.N., Mittelbronn, M., Antoniello, K., Paganetti, P., Muhs, A., Heilemann, M., Hawkins, R.A., Schrattenholz, A., Liebner, S., 2016. BACE-1 is expressed in the blood-brain barrier endothelium and is upregulated in a murine model of Alzheimer's disease. J. Cereb. Blood Flow Metab. 36, 1281–1294. https://doi.org/10.1177/0271678X15606463.

Devraj, K., Guérit, S., Macas, J., Reiss, Y., 2018. An in vivo blood-brain barrier permeability assay in mice using fluorescently labeled tracers. J Vis Exp e57038–e57038. https://doi.org/10.3791/57038.

Duncan, R.N., Xie, Y., McPherson, A.D., Taibi, A.V., Bonkowsky, J.L., Douglass, A.D., Dorsky, R.I., 2016. Hypothalamic radial glia function as self-renewing neural progenitors in the absence of Wnt/β-catenin signaling. Development 143, 45–53. https://doi.org/10.1242/dev.126813.

Eubelen, M., Bostaille, N., Cabochette, P., Gauquier, A., Tebabi, P., Dumitru, A.C., Koehler, M., Gut, P., Alsteens, D., Stainier, D.Y.R., Garcia-Pino, A., Vanhollebeke, B., 2018. A molecular mechanism for Wnt ligand-specific signaling. Science 361. https://doi.org/10.1126/science.aat1178 eaat1178.

Fisher, J., Devraj, K., Ingram, J., Slagle-Webb, B., Madhankumar, A.B., Liu, X., Klinger, M., Simpson, I.A., Connor, J.R., 2007. Ferritin: a novel mechanism for delivery of iron to the brain and other organs. Am. J. Physiol., Cell Physiol. 293, C641–9. https://doi.org/10.1152/ajpcell.00599.2006.

Fox, I.J., Paucar, A.A., Nakano, I., Mottahedeh, J., Dougherty, J.D., Kornblum, H.I., 2004. Developmental expression of glial fibrillary acidic protein mRNA in mouse forebrain germinal zones–implications for stem cell biology. Brain Res. Dev. Brain Res. 153, 121–125. https://doi.org/10.1016/j.devbrainres.2004.07.011.

Galbiati, F., Volonte, D., Brown, A.M.C., Weinstein, D.E., Ben-Ze'ev, A., Pestell, R.G., Lisanti, M.P., 2000. Caveolin-1 expression inhibits wnt/β-Catenin/Lef-1 signaling by recruiting β-Catenin to caveolae membrane domains. J. Biol. Chem. 275, 23368–23377. https://doi.org/10.1074/jbc.M002020200.

Garcia, A.D.R., Doan, N.B., Imura, T., Bush, T.G., Sofroniew, M.V., 2004. GFAP-expressing progenitors are the principal source of constitutive neurogenesis in adult mouse forebrain. Nat. Neurosci. 7, 1233–1241. https://doi.org/10.1038/nn1340.

Gupta, A., Gargiulo, A.T., Curtis, G.R., Badve, P.S., Pandey, S., Barson, J.R., 2018. Pituitary adenylate cyclase-activating Polypeptide-27 (PACAP-27) in the thalamic paraventricular nucleus is stimulated by ethanol drinking. Alcohol. Clin. Exp. Res. 42, 1650–1660. https://doi.org/10.1111/acer.13826.

Gurnik, S., Devraj, K., Macas, J., Yamaji, M., Starke, J., Scholz, A., Sommer, K., Di Tacchio, M., Vutukuri, R., Beck, H., Mittelbronn, M., Foerch, C., Pfeilschifter, W., Liebner, S., Peters, K.G., Plate, K.H., Reiss, Y., 2016. Angiopoietin-2-induced Blood-brain Barrier Compromise and Increased Stroke Size Are Rescued by VE-PTP-dependent Restoration of Tie2 Signaling, 131, pp. 753–773. https://doi.org/10.1007/s00401-016-1551-3.

Haseloff, R.F., Blasig, I.E., Bauer, H.C., Bauer, H., 2005. In search of the astrocytic factor (s) modulating blood–Brain barrier functions in brain capillary endothelial cells in vitro. Cell. Mol. Neurobiol. 25, 25–39. https://doi.org/10.1007/s10571-004-1375-x.

Janzer, R.C., Raff, M.C., 1987. Astrocytes induce blood-brain barrier properties in endothelial cells. Nature 325, 253–257. https://doi.org/10.1038/325253a0.

Junge, H.J., Yang, S., Burton, J.B., Paes, K., Shu, X., French, D.M., Costa, M., Rice, D.S., Ye, W., 2009. TSPAN12 regulates retinal vascular development by promoting Norrin- but not Wnt-induced FZD4/beta-catenin signaling. Cell 139, 299–311. https://doi.org/10.1016/j.cell.2009.07.048.

Kim, T.-K., Han, P.-L., 2016. Chronic stress and moderate physical exercise prompt widespread common activation and limited differential activation in specific brain regions. Neurochem. Int. 99, 252–261. https://doi.org/10.1016/j.neuint.2016.08.007.

Langmead, B., Salzberg, S.L., 2012. Fast gapped-read alignment with Bowtie 2. Nat. Methods 9, 357–359. https://doi.org/10.1038/nmeth.1923.

Lengfeld, J.E., Lutz, S.E., Smith, J.R., Diaconu, C., Scott, C., Kofman, S.B., Choi, C., Walsh, C.M., Raine, C.S., Agalliu, I., Agalliu, D., 2017. Endothelial Wnt/β-catenin signaling reduces immune cell infiltration in multiple sclerosis. Proc. Natl. Acad. Sci. 114, E1168–E1177. https://doi.org/10.1073/pnas.1609905114.

Lezzerini, M., Budovskaya, Y., 2014. A dual role of the Wnt signaling pathway during aging in Caenorhabditis elegans. Aging Cell 13, 8–18. https://doi.org/10.1111/acel.12141.

Liebner, S., Corada, M., Bangsow, T., Babbage, J., Taddei, A., Czupalla, C.J., Reis, M., Felici, A., Wolburg, H., Fruttiger, M., Taketo, M.M., Melchner von, H., Plate, K.H., Gerhardt, H., Dejana, E., 2008. Wnt/beta-catenin signaling controls development of the blood-brain barrier. J. Cell Biol. 183, 409–417. https://doi.org/10.1083/jcb.200806024.

Liebner, S., Czupalla, C.J., Wolburg, H., 2011. Current concepts of blood-brain barrier development. Int. J. Dev. Biol. 55, 467–476. https://doi.org/10.1387/ijdb.103224sl.

Lippmann, E.S., Weidenfeller, C., Svendsen, C.N., Shusta, E.V., 2011. Blood-brain barrier modeling with co-cultured neural progenitor cell-derived astrocytes and neurons. J. Neurochem. 119, 507–520. https://doi.org/10.1111/j.1471-4159.2011.07434.x.

Ma, S., Kwon, H.J., Johng, H., Zang, K., Huang, Z., 2013. Radial glial neural progenitors regulate nascent brain vascular network stabilization via inhibition of Wnt signaling. PLoS Biol. 11, e1001469 https://doi.org/10.1371/journal.pbio.1001469.

Manley, G.T., Fujimura, M., Ma, T., Noshita, N., Filiz, F., Bollen, A.W., Chan, P., Verkman, A.S., 2000. Aquaporin-4 deletion in mice reduces brain edema after acute water intoxication and ischemic stroke. Nat. Med. 6, 159–163. https://doi.org/10.1038/72256.

Mátyás, F., Lee, J., Shin, H.-S., Acsády, L., 2014. The fear circuit of the mouse forebrain: connections between the mediodorsal thalamus, frontal cortices and basolateral amygdala. Eur. J. Neurosci. 39, 1810–1823. https://doi.org/10.1111/ejn.12610.

Mesic, I., Guzman, Y.F., Guedea, A.L., Jovasevic, V., Corcoran, K.A., Leaderbrand, K., Nishimori, K., Contractor, A., Radulovic, J., 2015. Double dissociation of the roles of metabotropic glutamate receptor 5 and oxytocin receptor in discrete social behaviors. Neuropsychopharmacology 40, 2337–2346. https://doi.org/10.1038/npp.2015.81.

Moon, Y., Kim, H.J., Kim, J.Y., Kim, H., Kim, W.R., Sun, W., 2011. Different expression of human GFAP promoter-derived GFP in different subsets of astrocytes in the mouse brain. Animal Cells Syst. (Seoul) 15, 268–273. https://doi.org/10.1080/19768354.2011.611254.

Morita, N., Nakahira, K., Baba, H., Akita, H., Kumada, T., Ogawa, M., Nakajima, K., Kawata, M., Mikoshiba, K., Ikenaka, K., 1997. Astrocytic lineage analysis by detection of GFAP promoter activity in vitro. Dev. Neurosci. 19, 210–218. https://doi.org/10.1159/000111208.

Muzumdar, M.D., Tasic, B., Miyamichi, K., Li, L., Luo, L., 2007. A global double-fluorescent Cre reporter mouse. Genesis 45, 593–605. https://doi.org/10.1002/dvg.20335.

Nagelhus, E.A., Mathiisen, T.M., Ottersen, O.P., 2004. Aquaporin-4 in the central nervous system: cellular and subcellular distribution and coexpression with KIR4.1. NSC 129, 905–913. https://doi.org/10.1016/j.neuroscience.2004.08.053.

Nold-Petry, C.A., Lo, C.Y., Rudloff, I., Elgass, K.D., Li, S., Gantier, M.P., Lotz-Havla, A.S., Gersting, S.W., Cho, S.X., Lao, J.C., Ellisdon, A.M., Rotter, B., Azam, T., Mangan, N. E., Rossello, F.J., Whisstock, J.C., Bufler, P., Garlanda, C., Mantovani, A., Dinarello, C.A., Nold, M.F., 2015. IL-37 requires the receptors IL-18Rα and IL-1R8 (SIGIRR) to carry out its multifaceted anti-inflammatory program upon innate signal transduction. Nat. Immunol. 16, 354–365. https://doi.org/10.1038/ni.3103.

Paganetti, P., Antoniello, K., Devraj, K., Toni, N., Kieran, D., Madani, R., Pihlgren, M., Adolfsson, O., Froestl, W., Schrattenholz, A., Liebner, S., Havas, D., Windisch, M., Cirrito, J.R., Pfeifer, A., Muhs, A., 2014. Increased efflux of amyloid-β peptides through the blood-brain barrier by muscarinic acetylcholine receptor inhibition reduces pathological phenotypes in mouse models of brain amyloidosis. J. Alzheimers Dis. 38, 767–786. https://doi.org/10.3233/JAD-131091.

Paolinelli, R., Corada, M., Ferrarini, L., Devraj, K., Artus, C., Czupalla, C.J., Rudini, N., Maddaluno, L., Papa, E., Engelhardt, B., Couraud, P.-O., Liebner, S., Dejana, E., 2013. Wnt activation of immortalized brain endothelial cells as a tool for generating a standardized model of the blood brain barrier in vitro. PLoS One 8, e70233. https://doi.org/10.1371/journal.pone.0070233.s008.

Paydar, A., Lee, B., Gangadharan, G., Lee, S., Hwang, E.M., Shin, H.-S., 2014. Extrasynaptic GABAA receptors in mediodorsal thalamic nucleus modulate fear extinction learning. Mol. Brain 7, 39. https://doi.org/10.1186/1756-6606-7-39.

Penzo, M.A., Robert, V., Tucciarone, J., De Bundel, D., Wang, M., Van Aelst, L., Darvas, M., Parada, L.F., Palmiter, R.D., He, M., Huang, Z.J., Li, B., 2015. The paraventricular thalamus controls a central amygdala fear circuit. Nature 519, 455–459. https://doi.org/10.1038/nature13978.

Posokhova, E., Shukla, A., Seaman, S., Volate, S., Hilton, M.B., Wu, B., Morris, H., Swing, D.A., Zhou, M., Zudaire, E., Rubin, J.S., St Croix, B., 2015. GPR124 functions as a WNT7-specific coactivator of canonical β-catenin signaling. CellReports 10, 123–130. https://doi.org/10.1016/j.celrep.2014.12.020.

Qian, X., Shen, Q., Goderie, S.K., He, W., Capela, A., Davis, A.A., Temple, S., 2000. Timing of CNS cell generation: a programmed sequence of neuron and glial cell production from isolated murine cortical stem cells. Neuron 28, 69–80.

Reis, M., Liebner, S., 2013. Wnt signaling in the vasculature. Exp. Cell Res. 319, 1317–1323. https://doi.org/10.1016/j.yexcr.2012.12.023.

Sato, A., Yamamoto, H., Sakane, H., Koyama, H., Kikuchi, A., 2010. Wnt5a regulates distinct signalling pathways by binding to Frizzled2. EMBO J. 29, 41–54. https://doi.org/10.1038/emboj.2009.322.

Saubaméa, B., Cochois-Guégan, V., Cisternino, S., Scherrmann, J.-M., 2012. Heterogeneity in the rat brain vasculature revealed by quantitative confocal analysis of endothelial barrier antigen and P-glycoprotein expression. J. Cereb. Blood Flow Metab. 32, 81–92. https://doi.org/10.1038/jcbfm.2011.109.

Saunders, N.R., Dreifuss, J.-J., Dziegielewska, K.M., Johansson, P.A., Habgood, M.D., Møllgård, K., Bauer, H.-C., 2014. The rights and wrongs of blood-brain barrier permeability studies: a walk through 100 years of history. Front. Neurosci. 8, 404. https://doi.org/10.3389/fnins.2014.00404.

Stenman, J.M., Rajagopal, J., Carroll, T.J., Ishibashi, M., McMahon, J., McMahon, A.P., 2008. Canonical Wnt signaling regulates organ-specific assembly and differentiation of CNS vasculature. Science 322, 1247–1250. https://doi.org/10.1126/science.1164594.

Talishinsky, A., Rosen, G.D., 2012. Systems genetics of the lateral septal nucleus in mouse: heritability, genetic control, and covariation with behavioral and morphological traits. PLoS One 7, e44236. https://doi.org/10.1371/journal.pone.0044236.

Uliasz, T.F., Hamby, M.E., Jackman, N.A., Hewett, J.A., Hewett, S.J., 2012. Generation of primary astrocyte cultures devoid of contaminating microglia. Methods Mol. Biol. 814, 61–79. https://doi.org/10.1007/978-1-61779-452-0_5.

Vallon, M., Yuki, K., Nguyen, T.D., Chang, J., Yuan, J., Siepe, D., Miao, Y., Essler, M., Noda, M., Garcia, K.C., Kuo, C.J., 2018. A RECK-WNT7 receptor-ligand interaction enables isoform-specific regulation of wnt bioavailability. CellReports 25, 339–349. https://doi.org/10.1016/j.celrep.2018.09.045 e9.

Vanhollebeke, B., Stone, O.A., Bostaille, N., Cho, C., Zhou, Y., Maquet, E., Gauquier, A., Cabochette, P., Fukuhara, S., Mochizuki, N., Nathans, J., Stainier, D.Y., 2015. Tip cell-specific requirement for an atypical Gpr124- and Reck-dependent Wnt/β-catenin pathway during brain angiogenesis. Elife 4, e06489. https://doi.org/10.7554/eLife.06489.

Vanlandewijck, M., He, L., Mäe, M.A., Andrae, J., Ando, K., Del Gaudio, F., Nahar, K., Lebouvier, T., Laviña, B., Gouveia, L., Sun, Y., Raschperger, E., Räsänen, M., Zarb, Y., Mochizuki, N., Keller, A., Lendahl, U., Betsholtz, C., 2018. A molecular atlas of cell types and zonation in the brain vasculature. Nature. https://doi.org/10.1038/nature25739.

Walter, W., Sánchez-Cabo, F., Ricote, M., 2015. GOplot: an R package for visually combining expression data with functional analysis. Bioinformatics 31, 2912–2914. https://doi.org/10.1093/bioinformatics/btv300.

Wang, L., Feng, Z., Wang, X., Wang, X., Zhang, X., 2010. DEGseq: an R package for identifying differentially expressed genes from RNA-seq data. Bioinformatics 26, 136–138. https://doi.org/10.1093/bioinformatics/btp612.

Wang, Y., Sabbagh, M.F., Gu, X., Rattner, A., Williams, J., Nathans, J., 2019. Beta-catenin signaling regulates barrier-specific gene expression in circumventricular organ and ocular vasculatures. Elife 8, 3221. https://doi.org/10.7554/eLife.43257.

Weidenfeller, C., Svendsen, C.N., Shusta, E.V., 2007. Differentiating embryonic neural progenitor cells induce blood-brain barrier properties. J. Neurochem. 101, 555–565. https://doi.org/10.1111/j.1471-4159.2006.04394.x.

Wu, Y., Zhang, A.-Q., Yew, D.T., 2005. Age related changes of various markers of astrocytes in senescence-accelerated mice hippocampus. Neurochem. Int. 46, 565–574. https://doi.org/10.1016/j.neuint.2005.01.002.

Yamamoto, H., Komekado, H., Kikuchi, A., 2006. Caveolin is necessary for Wnt-3a-Dependent internalization of LRP6 and accumulation of β-Catenin. Dev. Cell 11, 213–223. https://doi.org/10.1016/j.devcel.2006.07.003.

Yao, Y., Sun, S., Wang, J., Fei, F., Dong, Z., Ke, A.-W., He, R., Wang, L., Zhang, L., Ji, M.-B., Li, Q., Yu, M., Shi, G.-M., Fan, J., Gong, Z., Wang, X., 2018. Canonical wnt signaling remodels lipid metabolism in zebrafish hepatocytes following ras oncogenic insult. Cancer Res. 78, 5548–5560. https://doi.org/10.1158/0008-5472.CAN-17-3964.

Ye, X., Wang, Y., Cahill, H., Yu, M., Badea, T.C., Smallwood, P.M., Peachey, N.S., Nathans, J., 2009. Norrin, frizzled-4, and Lrp5 signaling in endothelial cells controls a genetic program for retinal vascularization. Cell 139, 285–298. https://doi.org/10.1016/j.cell.2009.07.047.

Zhang, Y., Chen, K., Sloan, S.A., Bennett, M.L., Scholze, A.R., O'Keeffe, S., Phatnani, H.P., Guarnieri, P., Caneda, C., Ruderisch, N., Deng, S., Liddelow, S.A., Zhang, C., Daneman, R., Maniatis, T., Barres, B.A., Wu, J.Q., 2014. An RNA-Sequencing transcriptome and splicing database of glia, neurons, and vascular cells of the cerebral cortex. J. Neurosci. 34, 11929–11947. https://doi.org/10.1523/JNEUROSCI.1860-14.2014.

Zhou, Y., Nathans, J., 2014. Gpr124 controls CNS angiogenesis and blood-brain barrier integrity by promoting ligand-specific canonical wnt signaling. Dev. Cell 31, 248–256. https://doi.org/10.1016/j.devcel.2014.08.018.

Zhou, Y., Wang, Y., Tischfield, M., Williams, J., Smallwood, P.M., Rattner, A., Taketo, M. M., Nathans, J., 2014a. Canonical WNT signaling components in vascular development and barrier formation. J. Clin. Invest. 124, 3825–3846. https://doi.org/10.1172/jci76431.

Zhou, Y., Wang, Y., Tischfield, M., Williams, J., Smallwood, P.M., Rattner, A., Taketo, M. M., Nathans, J., 2014b. Canonical WNT signaling components in vascular development and barrier formation. J. Clin. Invest. 124, 3825–3846. https://doi.org/10.1172/JCI76431.